



Article

π - π -Stacked Poly(ϵ -caprolactone)-*b*-poly(ethylene glycol) Micelles Loaded with a Photosensitizer for Photodynamic Therapy

Yanna Liu ¹, Marcel H.A.M. Fens ¹, Bo Lou ¹ , Nicky C.H. van Kronenburg ¹,
Roel F.M. Maas-Bakker ¹, Robbert J. Kok ¹, Sabrina Oliveira ^{1,2} , Wim E. Hennink ¹ and
Cornelus F. van Nostrum ^{1,*}

¹ Department of Pharmaceutics, Utrecht Institute for Pharmaceutical Sciences, Utrecht University, Universiteitsweg 99, 3508 TB Utrecht, The Netherlands; y.liu7@uu.nl (Y.L.); m.h.a.m.fens@uu.nl (M.H.A.M.F.); B.Lou@uu.nl (B.L.); n.c.h.vankronenburg@uu.nl (N.C.H.v.K.); r.maas@uu.nl (R.F.M.M.-B.); R.J.Kok@uu.nl (R.J.K.); S.Oliveira@uu.nl (S.O.); W.E.Hennink@uu.nl (W.E.H.)

² Division of Cell Biology, Neurobiology and Biophysics, Department of Biology, Utrecht University, Padualaan 8, 3584 CH Utrecht, The Netherlands

* Correspondence: C.F.vannostrum@uu.nl; Tel.: +31-620274607

Received: 13 March 2020; Accepted: 6 April 2020; Published: 9 April 2020



Abstract: To improve the *in vivo* stability of poly(ϵ -caprolactone)-*b*-poly(ethylene glycol) (PCL-PEG)-based micelles and cargo retention by π - π stacking interactions, pendant aromatic rings were introduced by copolymerization of ϵ -caprolactone with benzyl 5-methyl-2-oxo-1,3-dioxane-5-carboxylate (TMC-Bz). It was shown that the incorporation of aromatic rings yielded smaller micelles (18–30 nm) with better colloidal stability in PBS than micelles without aromatic groups. The circulation time of *i.v.* injected micelles containing multiple pendant aromatic groups was longer ($t^{1/2-\alpha}$: ~0.7 h; $t^{1/2-\beta}$: 2.9 h) than that of micelles with a single terminal aromatic group ($t^{1/2} < 0.3$ h). In addition, the *in vitro* partitioning of the encapsulated photosensitizer (meta-tetra(hydroxyphenyl)chlorin, mTHPC) between micelles and human plasma was favored towards micelles for those that contained the pendant aromatic groups. However, this was not sufficient to fully retain mTHPC in the micelles *in vivo*, as indicated by similar biodistribution patterns of micellar mTHPC compared to free mTHPC, and unequal biodistribution patterns of mTHPC and the host micelles. Our study points out that more detailed *in vitro* methods are necessary to more reliably predict *in vivo* outcomes. Furthermore, additional measures beyond π - π stacking are needed to stably incorporate mTHPC in micelles in order to benefit from the use of micelles as targeted delivery systems.

Keywords: polymer micelles; photodynamic therapy; *in vitro* release; circulation kinetics; biodistribution

1. Introduction

Photodynamic therapy (PDT) is a minimally invasive form of therapy that has been approved for treatment of various types of cancers, including head and neck tumors, basal cell carcinoma, cervical, endobronchial, esophageal, bladder, and gastric cancers [1,2]. Compared to conventional treatments, such as surgery, radiation and chemotherapy, PDT has important advantages, including reduced toxicity for healthy tissues, lack of drug resistance mechanisms, and favorable cosmetic outcomes. Furthermore, evidence of immune activation has been described after PDT, capable of leading to antitumor immunity [3,4]. PDT is based on a photochemical reaction between a light activatable molecule (i.e., photosensitizers (PS)), light, and molecular oxygen, which are harmless individually [1]. In combination, PS can be excited by light of the wavelength matching its absorption maximum

and can subsequently transfer its energy to molecular oxygen to yield singlet oxygen species (ROS), which are highly reactive with biomolecules present in cytoplasm or cell membranes, leading to cell death [5,6]. Effective cancer PDT is, however, hindered by some undesired properties in PS. Most PS molecules—including the clinically approved second generation PS, meta-tetra(hydroxyphenyl)chlorin (mTHPC)—are highly hydrophobic due to the extended delocalized aromatic π electron system. This promotes non-specific binding to cells, resulting in unspecific distribution of PS in healthy tissues (i.e., no selective accumulation of the PS in tumorous tissues), which can cause skin toxicity [7–9]. Moreover, the poor water solubility caused by the high hydrophobicity makes PS prone to aggregation in aqueous solutions, leading to lower ROS generation and decreased therapeutic efficacy [9–11].

Loading of PS in polymeric micelles is a promising approach to address these challenges [12]. Polymeric micelles are self-assembled nanostructures based on amphiphilic block copolymers formed in an aqueous solution and have been extensively investigated as drug delivery systems, particularly for the targeted delivery of hydrophobic drugs [13–16]. Polymeric micelles are characterized by a well-defined structure, containing a hydrophobic core and a hydrophilic shell. The micellar core has a high capacity to accommodate hydrophobic compounds, including photosensitizers, while the hydrophilic shell, which is mostly composed of poly(ethylene glycol) (PEG), can result in prolonged retention of polymeric micelles in the blood circulation by delaying their recognition and rapid uptake by the reticuloendothelial system (RES) [17–20]. In addition, micelles have customizable sizes ranging from 10 to 100 nm, which is favorable for the passively targeted delivery of loaded hydrophobic drugs to the aimed sites via the enhanced permeability retention (EPR) effect [21,22]. Previous research by our group showed that micelles based on poly(ϵ -caprolactone)-*b*-methoxy poly(ethylene glycol) (PCL-PEG) block copolymers can be loaded with the photosensitizer mTHPC with very high loading capacity [23]. However, in a recent study, we showed a rapid release of this PS in the circulation after i.v. administration of the mTHPC-loaded PCL-PEG-based micelles [24]. The poor stability in the circulation is currently considered a limitation for micelles for successful clinical applications [24–27]. This instability is most likely due to a combination of extraction of the cargo from the micelles and micellar destabilization resulting from a large dilution volume upon injection or binding of drug–polymer chains to blood components (e.g., albumin, lipoproteins) [28].

To overcome their inherent instability, physical interactions through π - π stacking have been investigated to enhance the stability of polymeric micelles. For example, Kataoka et al. previously reported that micelles consisting of poly(ethylene glycol)-poly(aspartate) block copolymers derived with multiple pendant 4-phenyl-1-butanol showed high paclitaxel retention in vivo [29]. Yang et al. demonstrated that paclitaxel-loaded micelles based on methoxy-poly(ethylene glycol)-*b*-poly(*N*-(2-benzoyloxypropyl)methacrylamide) (mPEG-*b*-p(HPMAM-Bz)) had a significantly prolonged circulation time, good drug retention, and enhanced tumor accumulation, which resulted in substantially improved antitumor efficacy that was attributed to noncovalent stacking interactions between Bz groups and aromatic groups present in the drug [30–32]. In another study, thermosensitive HPMAM-lactate-based micelles that contained HPMAM-Bz (~30 mol%) units as comonomers were used to encapsulate a hydrophobic PS (i.e., Si(sol)₂Pc, an axially solketal-substituted silicon phthalocyanine), showing enhanced loading capacity and significantly improved retention of PS during 9 days of storage in phosphate-buffered saline (PBS) at 37 °C as compared to Si(sol)₂Pc loaded in HPMAM-lactate-based micelles lacking the aromatic comonomers [33].

The abovementioned studies prompted us to stabilize PCL-PEG micelles in the current study by π - π stacking interactions through introduction of multiple pendant aromatic moieties in the hydrophobic core. To this end, aromatic rings were incorporated in the hydrophobic polymer chains by ring-opening copolymerization of ϵ -caprolactone (CL) with a benzyl-functionalized trimethylene carbonate, namely benzyl 5-methyl-2-oxo-1,3-dioxane-5-carboxylate (TMC-Bz). For comparison, PCL-PEG diblock copolymers without and with one aromatic unit at the terminal PCL chain end were synthesized. Then, mTHPC was selected as a model PS with high aromaticity and hydrophobicity, and was encapsulated in polymeric micelles that were prepared from the resulting block copolymers.

The effect of aromatic π - π stacking interaction on the loading capacity, possible PS aggregation in the micellar core, and stability of mTHPC-loaded micelles were studied. The photocytotoxicity of the micellar PS formulations was evaluated on both A431 and HeLa tumor cell lines by a 3-(4,5-dimethylthiazol-2-yl)-5-(3-carboxymethoxyphenyl)-2-(4-sulfophenyl)-2H-tetrazolium (MTS) assay. Importantly, blood circulation kinetics and biodistribution of the micelles and the incorporated mTHPC were studied and compared with free mTHPC in A431 tumor-bearing mice using fluorescence intensity measurements and high performance liquid chromatography analysis, respectively, while the biodistribution of micelles was also visualized by 2D fluorescence reflectance imaging to reveal the correlation behavior between the cargo and its host micelles.

2. Materials and Methods

2.1. General

The ϵ -caprolactone (CL), methoxy-poly(ethylene glycol) (mPEG-OH, 2000 g/mol), methanesulfonic acid (MSA, $\geq 99.0\%$), pyridine (99.8%), benzyl bromide (98%), and triethylamine (TEA) were obtained from Sigma-Aldrich (Zwijndrecht, The Netherlands). Phosphate-buffered saline (PBS, pH 7.4, containing 11.9 mM phosphates, 137 mM sodium chloride and 2.7 mM potassium chloride) was obtained from Fischer Bioreagents (Bleiswijk, The Netherlands). Standard regenerated cellulose dialysis tubing (Spectra/Por[®]6) with a molecular weight cutoff (MWCO) of 1 kDa was purchased from Spectrumlabs (Rancho Dominguez, CA, USA). Radioimmunoprecipitation assay (RIPA) lysis buffer (10 \times , 0.5 M Tris-HCl, pH 7.4, 1.5 M NaCl, 2.5% deoxycholic acid, 10% NP-40, 10 mM EDTA) was purchased from Merck KGaA (Darmstadt, Germany). The 2,2-Bis-thiomethyl-trimethylene carbonate (TTC) was kindly provided by Professor Zhiyuan Zhong (Soochow University, Suzhou, China). Human epidermoid carcinoma A431 and human cervical carcinoma HeLa cells were obtained from the American Type Culture Collection (ATCC, Manassas, VA, USA). All other solvents and reagents were obtained from Biosolve (Valkenswaard, The Netherlands). The mPEG-OH was azeotropically dried from toluene prior to use. Dichloromethane (DCM, peptide synthesis grade), toluene, and dimethylformamide (DMF) were dried over 4Å molecular sieves (Sigma-Aldrich, Zwijndrecht, The Netherlands) prior to use. All other reagents were used as received.

The $^1\text{H}/^{13}\text{C}$ -NMR spectra of the synthesized monomer and polymers were recorded using a Bruker NMR spectrometer (600 MHz, Bruker, Billerica, MA, USA). The different samples were dissolved in CDCl_3 at concentrations of approximately 15 mg/mL. Chemical shifts of residual solvent (CHCl_3 : δ 7.26 and 77 for proton and carbon spectrum, respectively) were used as the reference lines. Peak multiplicity is designated as s (singlet), d (doublet), t (triplet), and m (multiplet).

2.2. Synthesis of Monomer and Polymers

2.2.1. Synthesis of Monomer

Synthesis of Benzyl 2,2-bis(hydroxymethyl)propionate

Benzyl 2,2-bis(hydroxymethyl)propionate was synthesized as previously described (Scheme 1A) [34] and obtained as white needle crystals (47.8 g, yield: 67%) with a melting point of 73 °C (Figure S1A, Supplementary Materials). ^1H -NMR (600 MHz, CDCl_3): δ 7.38 (m, $\text{OCOCH}_2\text{C}_6\text{H}_5$), 5.21 (s, $\text{OCOCH}_2\text{C}_6\text{H}_5$), 3.95-3.72 (m, $\text{HOCH}_2\text{CCH}_2\text{OH}$), 1.09 (s, CCH_3). ^{13}C -NMR (150 MHz, CDCl_3): δ 175.2, 135.6, 128.6, 128.3, 127.8, 68.3, 66.7, 49.2, 17.1.

Synthesis of Benzyl 5-methyl-2-oxo-1,3-dioxane-5-carboxylate

Benzyl 5-methyl-2-oxo-1,3-dioxane-5-carboxylate (i.e., trimethylene carbonate functionalized by benzyl group (TMC-Bz)) was synthesized as previously described (Scheme 1A) [34]. The product was obtained as a white solid (40.6 g, yield: 97%) and further purified by recrystallization from ethyl

acetate prior to being used for polymerization. The product after recrystallization was composed of white needle crystals and its melting point shifted from 73 (before recrystallization) to 75 °C (Figure S1B, Supplementary Materials). ¹H-NMR (600 MHz, CDCl₃): δ 7.38 (m, OCOCH₂C₆H₅), 5.22 (s, OCOCH₂C₆H₅), 4.71(m, COOCH₂CCH₂OCO), 4.21 (m, COOCH₂CCH₂OCO), 1.33 (s, OCH₂CCH₃). ¹³C-NMR (150 MHz, CDCl₃): δ 170.9, 147.4, 134.7, 128.7, 128.2, 72.9, 67.9, 40.2, 17.6.

2.2.2. Synthesis of Polymers

2.2.2.1. Synthesis of P(CL/TMC-Bz)-PEG

A representative procedure for the synthesis of poly(ε-caprolactone)-*co*-poly(benzyl 5-methyl-2-oxo-1,3-dioxane-5-carboxylate)-*b*-poly(ethylene glycol) (P(CL/TMC-Bz)-PEG, Scheme 1B) was carried out as previously described [35,36]. Briefly, CL (342 mg, 3.0 mmol), TMC-Bz (750 mg, 3.0 mmol), and mPEG-OH (660 mg, 0.33 mmol) were dissolved in 7 mL dry DCM, followed by addition of MSA (37 mg, 0.39 mmol) with agitation. The reaction was allowed to proceed at 37 °C under N₂ atmosphere. At predetermined time points, samples were withdrawn from the reaction mixture and analyzed using ¹H-NMR spectroscopy to monitor monomer conversion in time, and thus the polymerization kinetics of CL and TMC-Bz. After 10 h, TEA (54 μL, 0.39 mmol; equimolar to MSA) was added to terminate the reaction. The cooled reaction solution was dropped into a 20-fold excess of cold diethyl ether (−20 °C) and the precipitate was collected by filtration and dried under vacuum to give the final product (entry 7 in Table 1).

PCL-PEG (Entries 1 and 5, Table 1) and P(TMC-Bz)-PEG (entry 3, Table 1) block copolymers were synthesized using MSA as the catalyst under the same conditions by polymerization of only CL or TMC-Bz, respectively.

The polymerization kinetics were determined by monitoring the decrease of peak integrals of methylene of CL at 2.66 ppm and methylene of benzyl group in TMC-Bz at 4.69 ppm. The peak originating from the three methoxy protons of mPEG-OH at 3.37 ppm was used as the reference peak to normalize the integrals.

2.2.2.2. Synthesis of Bz-PCL-PEG

To obtain benzylated PCL-PEG (Bz-PCL-PEG), the hydroxyl end groups of PCL-PEG were reacted with benzoyl chloride (Scheme 1C), as reported before [37]. In short, 1.2 g of PCL-PEG was dissolved in 6 mL dry DCM, which also contained a 5-fold molar excess of TEA compared to PCL-PEG. This solution was subsequently added dropwise to a solution of 5 equivalents of benzoyl chloride in 3 mL of dry DCM and stirred overnight under a nitrogen atmosphere. Finally, the solvent was removed under reduced pressure and the obtained residue was dissolved in DCM and purified by precipitation in an excess of diethyl ether (−20 °C). The collected precipitate of Bz-PCL-PEG was dried under vacuum and obtained as a white solid.

2.3. Polymer Characterization

The average degree of polymerization (DP) of CL or TMC-Bz in the obtained copolymers was determined by ¹H-NMR; that is, from the ratio of the integral of the CH₂ protons of the CL units (1.39 ppm, 2H, CH₂CH₂CH₂CH₂CH₂) or the CH₂ protons of benzyl groups in the poly(TMC-Bz) block (5.15 ppm, 2H, OCH₂C₆H₅) to the methyl protons of mPEG-OH (3.37 ppm, 3H, CH₃O), respectively. The number average molecular weight (M_n) of the block copolymers was calculated from the resulting DP of CL and TMC-Bz units and the molecular weight of the PEG block.

Gel permeation chromatography (GPC) analysis of the synthesized polymers was conducted to determine the number average molecular weight (M_n), weight average molecular weight (M_w), and polydispersity (PDI, equal to M_w/M_n) of the obtained block copolymers, using two PLgel Mesopore columns (300 × 7.5 mm, including a guard column, 50 × 7.5 mm) coupled with a differential refractive index (RI) detector. Poly(ethylene glycol)s of narrow molecular weights ranging from 430 to 26,100 g/mol

were used as calibration standards. The eluent was DMF containing 10 mM LiCl, the elution rate was 1.0 mL/min, and the temperature was set at 65 °C [24].

Differential scanning calorimetry (DSC) was carried out using a Discovery DSC (TA Instruments, New Castle, DE, USA) calibrated with indium. Samples (~5 mg) were heated with a ramp of 3 °C/min up to 150 °C (modulated), annealed for 5 min, cooled down at 3 °C/min to -80 °C (modulated), again annealed for 5 min, and subsequently heated at 3 °C/min up to 150 °C (modulated). Melting temperatures (T_m) were obtained from the onset of the peaks of the total heat flow and the melting enthalpies (ΔH_m) were recorded from the total heat flow. Glass transition temperatures (T_g) are defined as the point of inflection of the step change observed in the reversing heat flow curve. Data for the second heating cycle were recorded.

2.4. Synthesis and Characterization of Cy7-Labeled P(CL/TTC)-PEG

For *in vivo* studies, Cy7-labeled polymers were obtained by first synthesizing a block copolymer containing pendant thiol groups (i.e., poly(ϵ -caprolactone-*co*-2,2-bis-thiomethyl-trimethylene carbonate)-*b*-poly(ethylene glycol) (P(CL₁₈-TTC_{7.5})-PEG)), and allowing this polymer to react with maleimide-functionalized near-infrared (NIR) fluorophore Cyanine7 (Cy7) (Lumiprobe Corporation, Hannover, Germany), as described previously (Scheme S1, Supplementary Materials) [38]. In short, CL was copolymerized with TTC using mPEG-OH as an initiator and MSA as a catalyst (molar ratio of CL/TTC/mPEG-OH was 18/8/1), following the same procedure as described in Section 2.2.2.1 for the synthesis of P(CL/TMC-Bz)-PEG. Subsequently, the disulfide bonds in the resulting P(CL₁₈-TTC_{7.5})-PEG were reduced using tris(2-chloroethyl) phosphate (TCEP) to yield free thiol groups, which in turn were used for reaction with Cy7-maleimide (0.64 equivalent per polymer chain) via the thiol-maleimide reaction (Scheme S1, Supplementary Materials). After the reaction (4 h at room temperature), the unreacted free thiols were blocked by reaction with maleimide (4 h at room temperature), and subsequently, the unreacted maleimide and unreacted Cy7 were removed by dialysis against THF/water (50:50 volume ratio) for 3 days. The successful coupling of Cy7 with the polymer and complete removal of free Cy7 was demonstrated by GPC analysis, with which the amount of Cy7 in the copolymer was quantified using UV-Vis detection at 755.5 nm, showing 17% coupling efficiency, as reported previously [38]. On average, one polymer chain carried 0.17 Cy7 label.

2.5. Preparation and Characterization of Empty and mTHPC-Loaded Micelles

Empty micelles were prepared by a nanoprecipitation method, as previously described and with a slight modification [39]. In short, 10 mg of block copolymer was dissolved in dimethylsulfoxide (DMSO, 100 μ L). After vortexing for 1 min, the mixture was heated up to 70 °C for 5 min to obtain a homogenous solution. This warm solution was cooled down to room temperature and then added dropwise to PBS at 1:9 volume ratio. A homogenous micellar dispersion was formed after gentle shaking, followed by dialysis using tubing (MWCO = 1 kDa) against PBS at room temperature for 12 h. The micellar dispersion obtained after dialysis was filtered through a 0.2 μ m syringe filter. The Z-average hydrodynamic diameter (Z_{ave}) and polydispersity index (PDI) of the formed micelles after dialysis were determined by dynamic light scattering (DLS) at a fixed scattering angle of 173° and at 25 °C using a ZetaSizer Nano S (Malvern, Surrey, UK).

The mTHPC-loaded micelles (different loading percentages) were prepared as follows. A certain volume of mTHPC solution in DMSO (10 mg/mL added volume depending on the aimed wt% loading) was added to the weighted polymer, followed by addition of a certain volume of DMSO to obtain a final polymer concentration of 100 mg/mL. Subsequently, the procedures were the same as mentioned above (i.e., the mixture was heated and then added to PBS, followed by dialysis against PBS). The absorbance of the micellar dispersion diluted in DMSO was recorded at 651.5 nm using a UV-2450 Shimadzu spectrophotometer (Kyoto, Japan) and calibration was done using a series of standard solutions of

mTHPC in DMSO to determine the mTHPC loading [24]. The loading efficiency (LE) and loading capacity (LC) of mTHPC were calculated using the following Equations (1) and (2), respectively:

$$LE (\%) = \frac{mTHPC \text{ loaded (mg)}}{mTHPC \text{ in the feed (mg)}} \times 100\% \quad (1)$$

$$LC (\%) = \frac{mTHPC \text{ loaded (mg)}}{\text{polymer used (mg)} + mTHPC \text{ loaded (mg)}} \times 100\% \quad (2)$$

2.6. Aggregation State of mTHPC

The mTHPC-loaded micelles with different loadings of mTHPC were prepared in PBS, as described in Section 2.5. The micellar dispersions were diluted 10 times in PBS (the final polymer concentration was 1 mg/mL). The fluorescence intensity of mTHPC was recorded using a Jasco FP8300 spectrofluorometer (Tokyo, Japan) at 655 nm (excitation at 420 nm) and plotted against the concentration of mTHPC loaded in the micelles.

2.7. In Vitro Release of mTHPC-Loaded Micelles in Human Plasma

The in vitro release of mTHPC-loaded micelles with 5 wt% mTHPC loading (prepared in PBS as described in Section 2.5) was studied in human plasma at 37 °C by monitoring the change of fluorescence intensity of mTHPC, as previously reported [24]. Foscan[®] (i.e., free mTHPC solution in ethanol/propylene glycol (40:60, w/w)) was used as a reference. In short, different formulations were added to human plasma at a volume ratio of 1:9. As controls, samples were diluted with PBS (1:9, v/v). After incubation at 37 °C, samples were taken at different time points (5 min, and 0.5, 1, 1.5, 2, 3, 5, 8 h) and pipetted into the wells of a 384-well plate to record the fluorescence intensity, as described in Section 2.6.

In addition, samples of Foscan[®] and micellar mTHPC formulation were taken after incubation with human plasma (1:9, v/v) at 37 °C for 5 h, and then 1.5, 2, 4, and 30 times diluted with either human plasma or PBS. After incubation at 37 °C, samples were taken at 0.5, 1, and 2 h and transferred into a 384-well plate to record the fluorescence intensity.

2.8. Dark Cytotoxicity and Photo-Cytotoxicity of Empty and mTHPC-Loaded Micelles

A431 and HeLa cells were cultured in Dulbecco's modified Eagle's medium (DMEM) containing glucose (1 g/L for A431 and 4.5 g/L for HeLa) and supplemented with 10% (v/v) fetal bovine serum (FBS). The cells were kept in culture at 37 °C in a humidified 5% CO₂ atmosphere.

Dispersions of empty and mTHPC-loaded micelles (with various loadings) were prepared in PBS (10 mg/mL polymer), as described in Section 2.5. The stock dispersions were diluted in DMEM medium (2.5 and 5 times dilution for empty micelles and 10 times dilution for the mTHPC-loaded micelles) prior to cell exposure for evaluation of their cytotoxicity (empty micelles), dark cytotoxicity, and photo-cytotoxicity (mTHPC-loaded micelles) on A431 and HeLa cells.

The cells were seeded into 96-well plates at a density of 6000 A431 cells/well or 5000 HeLa cells/well and incubated overnight at 37 °C and 5% CO₂. Subsequently, the medium (100 µL) in the wells was replaced by 100 µL of the above-described empty or mTHPC-loaded micellar dispersions. To evaluate the photocytotoxicity of the different micellar mTHPC formulations, the cells were incubated first in the dark for 7 h at 37 °C and 5% CO₂ with the different formulations. Next, the medium with the formulations was removed and cells were washed three times with DMEM medium. Subsequently, the cells in 100 µL of fresh DMEM were illuminated for 10 min with a light intensity of 3.5 mW/cm² (corresponding to 2.1 J/cm²), using a homemade device consisting of 96 LED lamps (650 ± 20 nm, 1 LED per well), and then incubated overnight at 37 °C and 5% CO₂. Finally, cell viability was measured as described before [24], by recording the absorbances of the different wells at 490 nm after the cells were exposed for

approximately 1 h to a CellTiter 96[®] AQueous One Solution (Promega, Leiden, The Netherlands) containing 3-(4,5-dimethylthiazol-2-yl)-5-(3-carboxymethoxyphenyl)-2-(4-sulfophenyl)-2H-tetrazolium (i.e., MTS assay).

For determination of the cytotoxicity of empty polymeric micelles (without mTHPC loading) and dark toxicity of the above described mTHPC-loaded micelles, the cells were incubated with the different formulations in the dark for 24 h at 37 °C and 5% CO₂, and subsequently the cell viability was determined directly (without irradiation) by the MTS assay after washing off the formulations [24].

2.9. In Vivo Studies of mTHPC and Micelles in A431 Tumor-Bearing Mice

For the in vivo studies, P(CL_{9,1}-TMC-Bz_{7,7})-PEG and Bz-PCL_{17,6}-PEG micelles loaded with mTHPC (0.6 wt% loading) were used and prepared as described in Section 2.5, except that micelles were labeled by mixing the block copolymer with Cy7-labeled P(CL₁₈-TTC_{7,5})-PEG (at a ratio of 98.5% to 1.5% *w/w*). A formulation of free mTHPC was prepared by 1:1 dilution of a 120 µg/mL mTHPC stock solution in Foscan[®] solvent (i.e., ethanol/propylene glycol, 40/60 *w/w*) with PBS (final mTHPC concentration was 60 µg/mL, corresponding to an equal dose of injected mTHPC as micellar formulation).

The animal experiments were approved by the Central Animal Experiments Committee (approval number #AVD108002016544) and the Animal Welfare Body Utrecht (approval number WP# 544-2-04). Female Balb/c nude mice, weighing 20–28 g, were purchased from Envigo (Horst, The Netherlands). Mice were housed in ventilated cages at 25 °C and 55% humidity under natural light/dark conditions. Food and water were provided ad libitum during the entire study. Mice were inoculated with 1×10^6 A431 cells suspended in 100 µL PBS subcutaneously into the right flank. When the tumors reached an approximate size of 100–300 mm³ (between 7 and 14 days after injection of the tumor cells), mice were included in the studies. Tumors were measured using a digital caliper. The tumor volume *V* (in mm³) was calculated using the equation $V = (\pi/6)LS^2$, in which *L* is the largest and *S* is the smallest superficial diameter [30].

2.9.1. Circulation Kinetics

Three groups of tumor-bearing mice (*n* = 4–6 per group) were intravenously (i.v.) injected via the tail vein with free mTHPC formulation (i.e., mTHPC dissolved in diluted Foscan solvent (ethanol/propylene glycol/PBS 20:30:50 *v/v/v*)) or Cy7-labeled mTHPC micelles, respectively, at injection doses of 300 µg mTHPC/kg, corresponding to ~6 µg mTHPC in ~120 µL per individual mouse with average body weight of ~25 g.

Blood samples were collected in tubes with EDTA anticoagulant via submandibular puncture (~60 µL) from mice at 1 min (100% injection control), then at 1 and 2 h, and via cardiac puncture (~200 µL) at 4 or 24 h post-injection. For the latter, mice were killed through cervical dislocation while under deep isoflurane anesthesia. The collected blood samples were centrifuged at 1000× *g* for 15 min at 4 °C. The plasma supernatant was collected, extracted using acetonitrile/DMSO (4:1, *v/v*), and analyzed by high-performance liquid chromatography (HPLC) and a LI-COR Odyssey imaging system to quantify the amount of mTHPC and Cy7-labeled micelles, respectively, as previously described [38]. Plasma concentration curves were analyzed by non-compartmental analysis with the PKSolver add-in for Microsoft Excel [40].

2.9.2. Biodistribution

The mice were sacrificed 4 (3–6 animals per group) or 24 h (3–6 animals per group) after i.v. administration of the formulations. Tumors and a panel of organs (spleen, liver, lung, heart, kidney, skin, femur, and brain) were excised and imaged *ex vivo* by 2D fluorescence reflectance imaging (FRI) using a Pearl Trilogy imager from LI-COR and then stored at –80 °C until further processing for quantification. Organs and tumors from three untreated animals were used as controls.

To quantify the content of mTHPC and micelles in the tumors and the different organs, the excised tissue samples were treated as follows. First, 100 µL of RIPA lysis buffer was added to 100 mg of

sliced tissues or organs. The mixture was homogenized by a tissue grinder (Perccellys 24) at a speed of 6000/s for 60 s (for femur samples, 6000/s for 180 s) and the homogenate was subsequently aliquoted. To determine the mTHPC concentration in the samples, 1 volume of an aliquot of the homogenate (30 μ L) was mixed with 120 μ L of acetonitrile/DMSO (4:1 *v/v*) and vortexed for 1 min. The mixture was then centrifuged at 15,000 \times *g* for 10 min. Next, 50 μ L of the obtained supernatant was injected into the HPLC system consisting of a Waters X Select Charged Surface Hybrid (CSH) C18 3.5 μ m 4.6 \times 150 mm column coupled with a fluorescence detector set at λ_{ex} 420 nm and λ_{em} 650 nm to analyze mTHPC concentration [38]. The mobile phase was 0.1 % trifluoroacetic acid in acetonitrile/water (60:40, *v/v*) at a flow rate of 1 mL/min. The measuring range was from 0.005 to 4 μ g/mL and the detection limit was 5 ng/mL. Calibration curves were obtained from a series of standard solutions of mTHPC in DMSO, to which 45 μ L of the corresponding homogenized tissue samples obtained from control mice (i.e., not treated with any formulations) was added, followed by mTHPC extraction using acetonitrile/DMSO (4:1, *v/v*) and HPLC analysis.

To determine the concentration of Cy7-labeled micelles in the tissue homogenates, 1 volume of another aliquot of the homogenate (30 μ L) was vortex-mixed with 2 volumes of RIPA lysis buffer (60 μ L) for 1 min. The fluorescence of Cy7 in the mixture (20 μ L) was detected at the 800 nm channel (i.e., λ_{ex} 785 nm and λ_{em} 820 nm), using a LI-COR Odyssey scanner imaging system, and a calibration curve was obtained using samples with different concentrations of Cy7-labeled copolymer in a mixture of RIPA buffer (1 volume) and the corresponding homogenized tumor or organ samples (2 volumes) obtained from non-treated mice.

It is noted that skin accumulation of different formulations was not included, as grinding of the skin was more problematic in our preliminary test, which could lead to unreliable quantification. In addition, a study by Bovis et al. suggested that mTHPC accumulation in the skin was limited [8].

2.10. Statistical Analysis

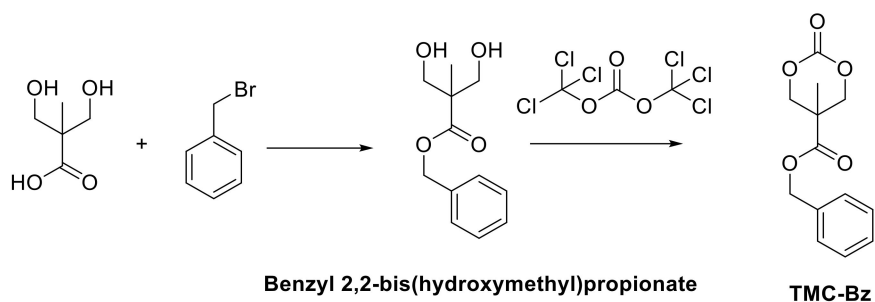
Statistical analysis was done by GraphPad Prism 8.3.0 software. Two-way analysis of variance (ANOVA) was used to determine the statistical significance of biodistribution among different mTHPC formulations. A value of $p < 0.05$ was considered significant. Statistical significance is depicted as * $p < 0.05$, ** $p < 0.01$, *** $p < 0.001$.

3. Results and Discussion

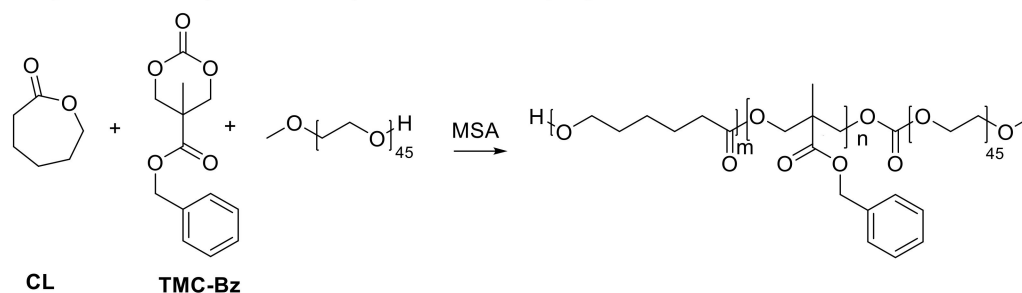
3.1. Synthesis and Characterization of Monomer and Polymers

To synthesize benzyl 5-methyl-2-oxo-1,3-dioxane-5-carboxylate (i.e., trimethylene carbonate functionalized by benzyl group, TMC-Bz), 2,2-bis(hydroxymethyl)propionate was first benzylated by reaction with benzyl bromide, followed by reaction with triphosgene (Scheme 1A). After purification, TMC-Bz was obtained in a high yield (97%) as a white crystalline solid. The structures of the intermediate product and TMC-Bz were confirmed by $^1\text{H}/^{13}\text{C}$ NMR spectroscopy (Figure S2, Supplementary Materials).

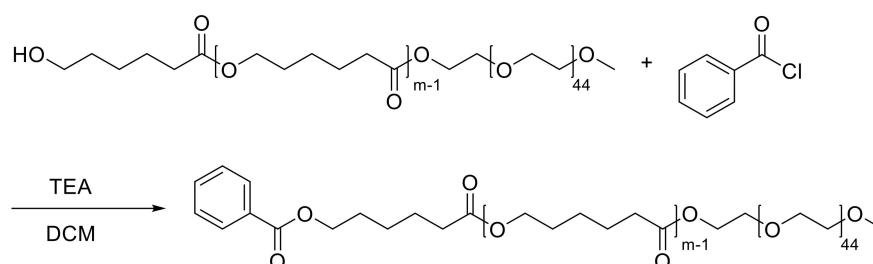
A. Synthesis of TMC-Bz



B. Synthesis of P(CL/TMC-Bz)-PEG block copolymer



C. Synthesis of Bz-PCL-PEG block copolymer



Scheme 1. Synthesis of benzyl 5-methyl-2-oxo-1,3-dioxane-5-carboxylate (TMC-Bz) (A), polymers of P(CL/TMC-Bz)-PEG (B), and Bz-PCL-PEG (C).

The block copolymers synthesized by the ring-opening polymerization of CL or TMC-Bz, initiated by mPEG-OH and catalyzed by MSA using different CL/TMC-Bz/initiator molar ratios (Scheme 1B), were obtained as white solids in a yield of ~65%, and their chemical structures were characterized by ^1H NMR (Figures S3–S5, Supplementary Materials). The characteristics of the obtained block copolymers are shown in Table 1. The compositions of the resulting block copolymers as determined by ^1H -NMR fit well with those expected from the ratios of the monomers in the feed. GPC analysis shows narrow molar mass distributions ($M_w/M_n \leq 1.1$), suggesting the absence of significant side reactions, such as transesterification [35,41–43]. For the ring-opening copolymerization of CL and TMC-Bz, similar polymerization rates of the two monomers were observed, as shown in Figure 1A for a CL/TMC-Bz/mPEG-OH feed molar ratio of 9:9:1 (i.e., entry 7, Table 1). The ^1H -NMR spectrum of the resulting block copolymer (Figure 1B) displayed three groups of peaks in the ester region at 3.90–4.40 ppm, corresponding to the three kinds of CH_2O -carbonyl linkages in the different diad structures that are present in the poly(ester-carbonate) block (i.e., TMC-Bz-TMC-Bz, CL-TMC-Bz, and CL-CL, respectively) [42,44]. This demonstrates a random distribution of CL and TMC-Bz in the

resulting P(CL/TMC-Bz)-PEG copolymers (entries 2, 4, 6, and 7, Table 1) which is in good agreement with the equal reactivity of the two monomers.

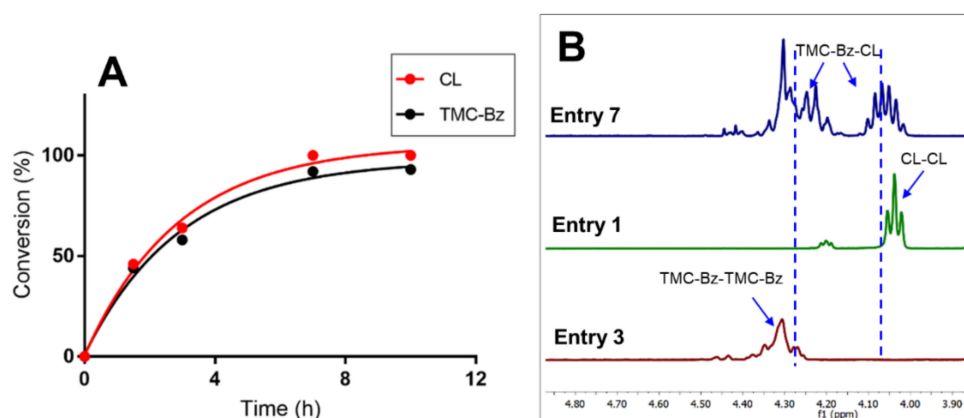


Figure 1. (A) Conversion of CL (red dots) and TMC-Bz (black dots) monitored by $^1\text{H-NMR}$ analysis as a function of time (entry 7, Table 1). (B) $^1\text{H-NMR}$ spectrum of the P(CL_{9,1}-TMC-Bz_{7,7})-PEG block copolymer (entry 7) in the region of methylene protons linked to oxy-carbonyl group (CH_2OCO), showing three different diad sequences in the copolymer. The spectra of PCL₉-PEG and P(TMC-Bz_{8,6})-PEG copolymers presented as entry 1 and 3 were used as references for assignments of the CL-CL and TMC-Bz-TMC-Bz diads, respectively. The entries presented in the legend correspond to the same entries in Table 1.

It is noted that the same characteristics of PCL_{17,6}-PEG and its terminal benzyl derivative (i.e., Bz-PCL_{17,6}-PEG) (entries 4 and 8, Table 1) indicate that loss of materials and undesired side reactions did not occur during the process of post-modification of the end groups (Scheme 1C). The assignments of the corresponding NMR peaks of Bz-PCL_{17,6}-PEG (Figure S6, Supplementary Materials) were in line with those reported previously [37]. In addition, the $^1\text{H-NMR}$ spectrum of Bz-PCL_{17,6}-PEG (Figure S6, Supplementary Materials) shows that the integral ratio of the protons of the terminal Bz group at 7–8 ppm to the terminal OCH_3 group of PEG at 3.37 ppm was 5:3 (corresponding with a molar ratio of Bz/ OCH_3 of 1:1), demonstrating that all polymer chains carry a terminal benzyl end group.

Table 1. Characteristics of the synthesized (Bz-)PCL-PEG and PCL/TMC-Bz)-PEG block copolymers.

Entry	Feed Ratio of CL/TMC-Bz/PEG (mol/mol/mol)	Composition of the Obtained Block Copolymers ^a	M_n ^b	M_w (GPC) ^c	M_n (GPC) ^c	M_w/M_n (GPC)	T_g (°C)	T_m (°C)	ΔH_m (J/g)
1	9/0/1	PCL ₉ -PEG	3.2	2.7	2.5	1.11	-	43	120
2	4.5/4.5/1	P(CL _{5,3} -TMC-Bz _{4,5})-PEG	3.9	2.7	2.5	1.06	-29	39	72
3	0/9/1	P(TMC-Bz _{8,6})-PEG	4.3	2.9	2.7	1.05	-12	35	82
4	4.5/9/1	P(CL _{4,8} -TMC-Bz _{9,2})-PEG	5.0	3.1	3.0	1.05	-11	32	64
5	18/0/1	PCL _{17,6} -PEG	4.2	2.9	2.7	1.09	-	42	107
6	14/4/1	P(CL _{13,5} -TMC-Bz _{3,7})-PEG	4.7	3.0	2.7	1.11	-47	38	89
7	9/9/1	P(CL _{9,1} -TMC-Bz _{7,7})-PEG	5.2	3.5	3.3	1.08	-19	39	67
8	-	Bz-PCL _{17,6} -PEG	4.3	2.9	2.7	1.09	-	40	110

^a Given numbers are degrees of polymerization of CL and TMC-Bz as determined by $^1\text{H-NMR}$; ^b determined by NMR; ^c calibration with PEG.

The thermal properties of the obtained block copolymers were investigated by DSC (Table 1, representative thermograms are shown in Figure S7, Supplementary Materials). All block copolymers showed only one T_m at around 40 °C, close to that of mPEG-OH (48 °C), which is in accordance with previous data [24,45]. For the copolymers, crystallinity (i.e., ΔH_m) of PEG corrected for its weight fraction in the corresponding polymer chains was well in accordance with that of the mPEG-OH (measured ΔH_m was 182 J/g) (Figure S8A, Supplementary Materials), demonstrating that in the solid state, PEG and the polyester/carbonate blocks were phase-separated in the crystalline PEG domain and

amorphous P(CL-TMC-Bz) (entries 2, 4, 6 and 7, Table 1) with T_g 's, ranging from -47 to -11 °C. These T_g 's can be described by the Fox equation (Figure S8B, Supplementary Materials), suggesting a random distribution of CL and TMC-Bz in the polymer chains, which is in line with that observed from NMR analysis (Figure 1B). These amorphous domains are obviously not miscible with PEG. The PCL-PEG block copolymers (entries 1, 5, and 8, Table 1) were almost fully crystalline: both PCL and PEG have their T_m 's around 45 °C [45], while the P(TMC-Bz)-PEG (entry 3, Table 1) block copolymer had T_g at -12 °C, which resulted from the P(TMC-Bz) block and is in reasonable agreement with the T_g of PTMC₈₀ (-25 °C) [35].

3.2. Preparation and Characterization of Polymeric Micelles

Empty polymeric micelles were prepared at a polymer concentration of 10 mg/mL using a nanoprecipitation method by dropping a polymer solution in DMSO into an excess of PBS followed by dialysis. DLS measurements (Figure 2A) demonstrate that PCL₉-PEG (entry 1, Table 1) without aromatic rings formed directly after dialysis micelles with a size of 27 nm and a PDI of ~ 0.3 , which was in the range observed previously for low molecular weight oligolactates-*b*-PEG and oligocaprolactones-*b*-PEG ($M_n < 1.8$ kDa) with unmodified hydroxide end groups [37,45]. Importantly, the size and PDI of the PCL₉-PEG micelles (Figure S9A,B, Supplementary Materials) further increased to ~ 80 nm (PDI ~ 0.4) during 24 h storage at room temperature, in combination with an increased derived count rate from 2000 to 6000 (Figure S9C, Supplementary Materials), demonstrating formation of aggregates, pointing to a low colloidal stability. Similarly, the larger PCL_{17.6}-PEG micelles (entry 5, Table 1) showed a size of ~ 600 nm with PDI of ~ 0.7 even directly after dialysis. On the other hand, micelles from the corresponding benzyl-terminated polymer (entry 8, Table 1) showed substantially decreased size and size distribution (23 nm with PDI of 0.3 , Figure 2A). This result is in accordance with our previous studies, in which it was demonstrated that micelles based on PCL₉-PEG with a benzyl end group showed smaller size (17 nm), lower PDI (< 0.1), and better stability than the non-benzylated polymer micelles [24,38].

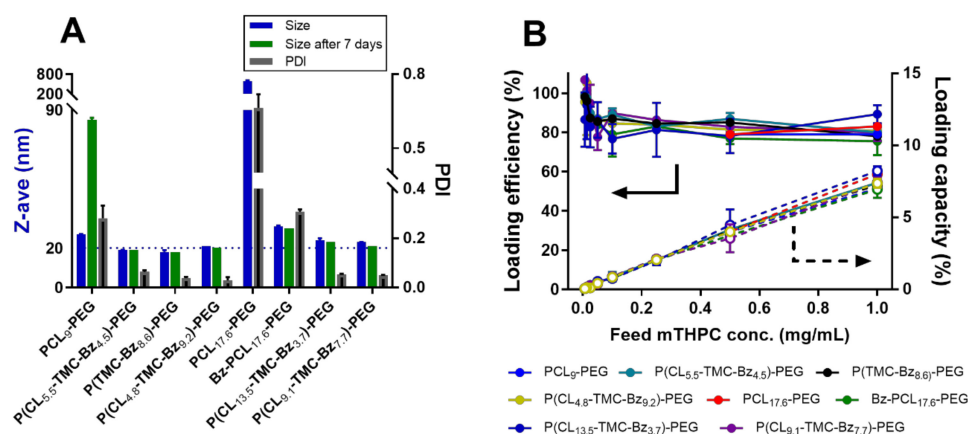


Figure 2. (A) Z-average hydrodynamic diameter (Z_{ave} , blue and green columns) and polydispersity index (PDI, black columns) of different empty polymeric micelles (10 mg/mL). (B) Loading efficiency and loading capacity of different micelles (10 mg/mL polymer) for mTHPC at various mTHPC feed concentrations.

Figure 2A shows that the different micelles based on P(CL/TMC-Bz)-PEG or P(TMC-Bz)-PEG block copolymers with different amounts of pendant benzyl groups (Entries 2–4, 6 and 7, Table 1) had small hydrodynamic diameters that slightly increased with the increasing chain length of the hydrophobic blocks (from 17 – 23 nm) with PDIs < 0.1 (Figure 2A). It is noted that the different aromatic substituted micelles, including Bz-PCL_{17.6}-PEG micelles, retained their small sizes and low PDIs for at least 7 days in PBS at room temperature (Figure 2A, green columns). Overall, these results demonstrate that aromatic groups, regardless of their positions and the amounts in the polymer chains, stabilized

the cores of micelles based on PCL-PEG. In addition, from the perspective of *in vivo* application, the relatively small sizes of these stable micelles are expected to favor both their accumulation in tumors through the EPR effect [21,22] and subsequent penetration into the tumor with uniform distribution, being crucial factors for anti-tumoral efficacy of nanomedicines [46–48].

The P(CL/TMC-Bz)-PEG and (Bz-)PCL-PEG-based micelles were loaded with mTHPC with loading efficiencies of $\geq 80\%$, as determined by UV-Vis analysis (Figure 2B, solid lines), independent of the composition of copolymers used, which led to a linear increase of loading capacity up to ~ 8 wt % with increasing mTHPC feed (Figure 2B, dash lines).

3.3. Aggregation State of mTHPC in Polymeric Micelles

The influence of the number of aromatic rings in the copolymers on the aggregation state of mTHPC in the different micelles was determined by measuring the quenching of its fluorescence [24,33,49]. For example, Yang et al. showed that the quenching concentration of a phthalocyanine (i.e., Si(sol)₂Pc) in aromatic-substituted thermosensitive micelles (0.45 mg/mL polymer) increased around 300 times to 16 $\mu\text{g/mL}$ compared to that in corresponding non-aromatic micelles (~ 0.05 $\mu\text{g/mL}$) [33]. As discussed in Section 3.2, polymeric micelles prepared from non-modified PCL-PEG copolymers showed low stability. Therefore, only the aromatic micelles with either benzyl-modified end groups or differing contents of benzyl pendant groups in the polymer chains were loaded with increasing amounts of mTHPC and the fluorescence intensity of mTHPC was measured. Figure 3A shows that the different mTHPC-loaded micelles exhibited similar fluorescence profiles. The fluorescence of mTHPC-loaded micelles increased almost linearly with increasing mTHPC loading from 0.06 to 0.5% *w/w* (i.e., ~ 0.6 to ~ 5 $\mu\text{g/mL}$ mTHPC; the final polymer concentration was 1 mg/mL). However, at higher loading percentages, mTHPC showed a rapid decrease in fluorescence intensity with increasing mTHPC loading, suggesting that fluorescence quenching resulting from mTHPC in the micelles occurred at ~ 10 $\mu\text{g/mL}$ (corresponding to 1 wt% mTHPC loading), in agreement with our previous work on mTHPC-loaded Bz-PCL-PEG micelles [24]. A higher maximum fluorescence was observed when mTHPC was loaded in P(CL/TMC-Bz)-PEG micelles with a high content of aromatic rings (i.e., molar ratio of PTMC-Bz/PCL in polymer chains > 0.3 ; Figure 3A, cyan, pink, yellow, and purple lines), because of the observed slightly later onset of quenching.

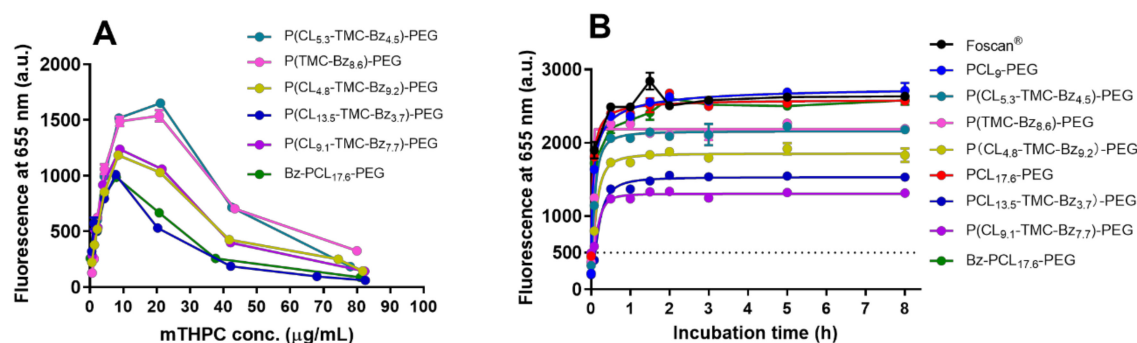


Figure 3. (A) Fluorescence intensity (λ_{ex} 420 nm, λ_{em} 655 nm) of various amounts of mTHPC loaded in different micelles; micelles of 10 mg/mL with different loading amounts (0.06–10% *w/w*) were individually prepared and each diluted 10 \times in PBS to obtain varying mTHPC concentrations. (B) Fluorescence intensity of Foscan[®] and mTHPC loaded in different micelles at a final mTHPC concentration of 40 $\mu\text{g/mL}$ (corresponding to 5wt% mTHPC feed loading in micelles) in human plasma as a function of time; Foscan[®] and mTHPC-loaded micelles were 10 \times diluted with full plasma and incubated, while the mTHPC fluorescence was recorded at 37 $^{\circ}\text{C}$ over a period of 8 h. The fluorescence intensities of the corresponding mTHPC-loaded micelles diluted with PBS were used as the 0 h timepoint.

3.4. In Vitro Release of mTHPC from Micelles in Human Plasma

The quenched state of the fluorescence when mTHPC is present in the micelles above 0.5% *w/w* loading (see Figure 3A) was used to investigate the in vitro stability of the mTHPC micellar formulations in human plasma [24]. When mTHPC is released from the micelles, this should lead to less quenching (i.e., increase in fluorescence intensity) as the local concentration inside the micelles is decreased, which is reinforced due to fluorescence of the free mTHPC likely bound to plasma proteins. For this purpose, the fluorescence of different micellar dispersion with 5wt% mTHPC feed loading, as well as mTHPC in its free form (Foscan[®]), was assessed in human plasma over time at 37 °C (Figure 3B). As expected, the fluorescence of mTHPC-loaded micelles upon 10× dilution in PBS did not change in time over 8 h at 37 °C (Supplementary Figure S10). Upon 10× dilution in plasma, Foscan[®] gave the highest immediate fluorescence, which increased slightly further during the first 30 min incubation and then remained stable at a value of ~2600 arbitrary units (a.u.); Figure 3B, black line). For all micellar mTHPC formulations (Figure 3B), substantial increase of fluorescence was observed to different levels within the first 1 h of incubation, and then the fluorescence intensities leveled off, reflecting different degrees of release of mTHPC from the micelles [24]. Interestingly, the plateau fluorescence intensities of mTHPC loaded in non-aromatic PCL₉-PEG or PCL_{17.6}-PEG micelles and Bz-PCL_{17.6}-PEG micelles (Figure 3B, blue, red, and green lines) were identical to that of Foscan[®] (at ~2600 a.u.), suggesting that the release was almost complete. This suggests that incorporating a single terminal aromatic group did not improve the retention of mTHPC in micelles in plasma, despite the enhanced colloidal stability of those micelles in PBS (see Figure 2A). In contrast, when mTHPC was loaded in micelles based on P(CL/TMC-Bz)-PEG or P(TMC-Bz)-PEG (i.e., with pendant aromatic rings), fluorescence intensities increased to lower levels than those loaded in the micelles from non-aromatic and chain-end modified polymers with a similar total length of hydrophobic blocks (Figure 3B, pink and cyan lines vs. blue line, or purple and dark blue lines vs. red and green lines). When the total length of hydrophobic blocks was kept more or less constant, the fluorescence intensity of mTHPC leveled off from 2600 a.u. (red line) to 1500 a.u. (dark blue line) and 1300 a.u. (purple line) as the content of TMC-Bz units increased from 0 to 4 and 8 units per polymer chain, respectively. On the other hand, when the degree of polymerization of TMC-Bz was ~8, the plateau fluorescence intensities of mTHPC were 2200 a.u. (pink line), 1800 a.u. (yellow line), and 1300 a.u. (purple line), with increasing total degree of polymerization (and thus molecular weight) of hydrophobic blocks from 8 to 14 and 17 units, respectively. Taken together, in plasma, mTHPC was most efficiently retained in micelles consisting of P(CL_{9.1}-TMC-Bz_{7.7})-PEG, which have the most TMC-Bz units and the longest hydrophobic blocks (Figure 3B, purple line). These results convincingly show that the retention of mTHPC in micelles was improved by pendant aromatic rings on the polymer backbone, while the extent of improvement depended on both the hydrophobic chain length and the number of aromatic moieties. The reported findings can be explained by the increased hydrophobic interactions and π - π stacking between the hydrophobic blocks of P(CL_{9.1}-TMC-Bz_{7.7})-PEG and mTHPC, which can to some extent prevent the extraction of the cargo from the micelles or the micellar destabilization resulting from the binding of mTHPC or amphiphilic polymer molecules with proteins such as albumin and lipoproteins present in human plasma.

To establish whether the observation of different plateau fluorescence levels of mTHPC-loaded micelles containing TMC-Bz is the result of simple equilibrium partitioning of mTHPC between micelles and plasma proteins, mTHPC-loaded P(CL_{9.1}-TMC-Bz_{7.7})-PEG micelles, after incubation with human plasma for 5 h, were further diluted with human plasma or PBS in different proportions and compared with Foscan[®] samples treated the same way. The solid black lines in Figure 4 show that upon further dilutions in human plasma, regardless of the dilution factors, the fluorescence of Foscan[®] samples was constant for 2 h and comparable to that observed upon dilution in PBS (broken black lines). The latter observation suggests that the amount of proteins present before further dilution was already sufficient to solubilize the amount of mTHPC that was present. When micelles were first incubated with plasma and subsequently diluted with PBS, the fluorescence intensity of mTHPC that was released from

the micelles did not change in time (Figure 4, broken purple lines) and remained lower than diluted Foscan[®], except for the highest dilution factor, which may point to further extraction of the PS from the micelles. Upon 1.5× dilution of the micelles with plasma instead of with PBS, the fluorescence intensity of mTHPC remained constant over time, which was again lower than the fluorescence intensity of the Foscan[®] sample (compare the solid purple line with the solid black line in Figure 4A). However, with further increase of the dilution factor of micelles in plasma to 2 and 4 times, the fluorescence of mTHPC in micelles showed an increase during the first 1 h incubation and then leveled off at different values (Figure 4B,C, solid purple lines). Upon 2× dilution in plasma, the plateau fluorescence was still lower than that observed from the corresponding Foscan[®] sample, while in the case of 4× dilution, the plateau fluorescence intensity of micellar mTHPC reached an identical level as observed in the Foscan[®] sample in plasma. Also, upon extensive dilution in plasma (30×), Foscan[®] and micellar mTHPC exhibited similar fluorescence levels (Figure 4D, purple lines). These results indicate that complete release of mTHPC from P(CL_{9,1}-TMC-Bz_{7,7})-PEG micelles was achieved when more plasma (≥4 times) was added. In other words, the equilibrium partitioning of mTHPC between micelles and plasma depends not only on the strength of the interaction with the polymer, but also on the ratio between micelles and plasma.

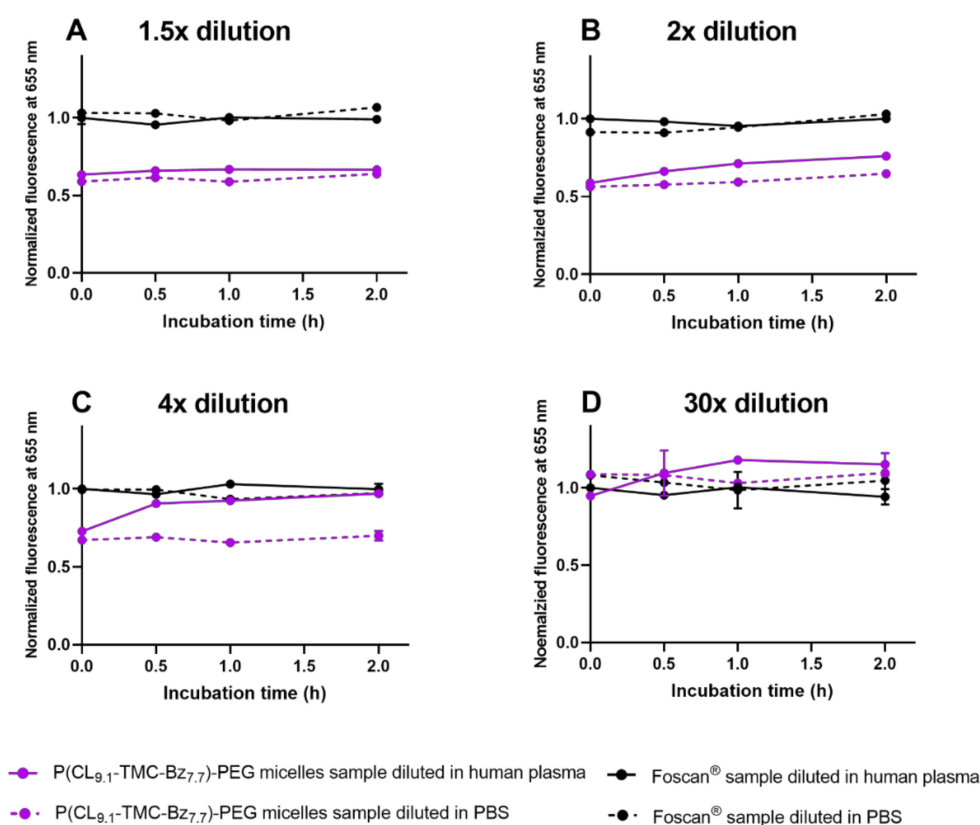


Figure 4. Fluorescence intensity of Foscan[®] and mTHPC-loaded P(CL_{9,1}-TMC-Bz_{7,7})-PEG micelles in human plasma and PBS as a function of time after dilution, normalized by the intensity of the corresponding Foscan[®] samples upon dilution with human plasma at 0 h; Foscan[®] and mTHPC-loaded micelles were pre-incubated with human plasma (1:9, v/v) at 37 °C for 5 h, then further diluted 1.5× (A), 2× (B), 4× (C), or 30× (D) with human plasma or PBS, and further incubated while the mTHPC fluorescence was recorded at 37 °C over a period of 2 h. The fluorescence intensities of mTHPC in different formulations recorded directly after dilution were used as the 0 h timepoint. The normalized fluorescence intensities were used because of a slight fluctuation of fluorescence intensity for different batches of samples, which showed an identical trend in a different independent experiment.

3.5. Dark Cytotoxicity and Photo-Cytotoxicity of Empty and mTHPC-Loaded Polymeric Micelles

Cell viability assays were performed on A431 and HeLa tumor cell lines to assess the cytocompatibility of the empty micellar formulations and to determine the dark toxicity and photo-toxicity of mTHPC-loaded micelles. These experiments were carried out with micelles based on Bz-PCL_{17.6}-PEG and three micelles based on polymers with pendant aromatic groups (i.e., P(CL/TMC-Bz)-PEG) with different PCL/PTMC-Bz ratios. Although all used micelles showed required colloidal stability in PBS (Figure 2A), the latter displayed better stability in human plasma (Figure 3B), as shown in Sections 3.2 and 3.4. Figure S11 (Supplementary Materials) shows that both A431 and HeLa cells incubated with empty micelles retained their viability at polymer concentrations up to 4 mg/mL, demonstrating that the different micelles have excellent cytocompatibility. As shown in Figure 5A,B, mTHPC-loaded in these different micelles, even with the highest mTHPC concentration up to 81 µg/mL, showed no cytotoxicity on A431 and HeLa cells after incubation with cells in the dark for 24 h. However, we showed before that free mTHPC (i.e., Foscan[®]) was toxic to cells without illumination at mTHPC concentrations higher than 50 µg/mL after 7 h and 20 µg/mL after 24 h [38]. This markedly decreased dark cytotoxicity of mTHPC by loading in the micelles is in line with previous observations using other micellar and liposomal formulations of mTHPC [50–52].

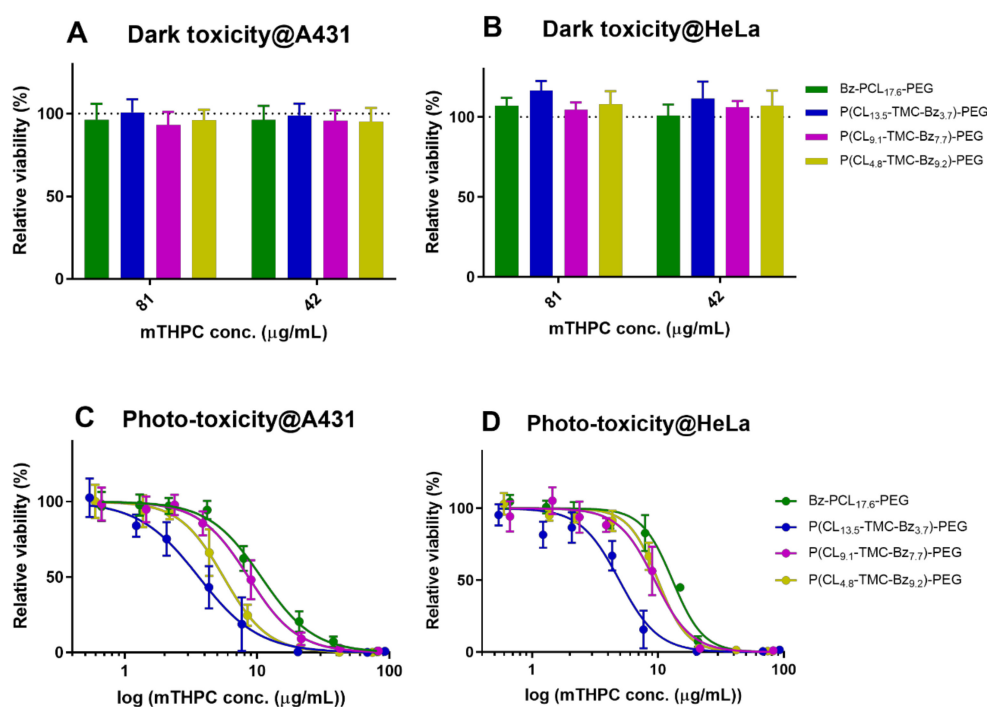


Figure 5. (A,B) Dark-toxicity established using cytotoxicity MTS assay of mTHPC loaded in micelles consisting of Bz-PCL-PEG and P(CL-TMC-Bz)-PEG (i.e., entries 4 and 6–8 from Table 1) at 1 mg/mL polymer and two different mTHPC loadings (10 wt% and 5wt% feeding, respectively) on A431 and HeLa cells after 24 h. (C,D) Dose-dependent photocytotoxicity (MTS assay) on A431 and HeLa cells after 7 h of pre-incubation with a series of mTHPC-loaded micelles; micelles of 10 mg/mL with different loading amounts were individually prepared and each was diluted 10× in DMEM to obtain the corresponding mTHPC concentrations. After the pre-incubation period and washing, the cells were illuminated for 10 min at 3.5 mW/cm².

The observed lack of dark toxicity could have been the result of no uptake of the micelles. However, our previous studies showed that PCL-PEG-based micellar mTHPC formulations and free mTHPC can both be effectively taken up by cells [38]. Indeed, photocytotoxicity studies (Figure 5C,D) show that the different micellar mTHPC formulations were able to induce cell killing upon irradiation and exhibited comparable cytotoxic effects on A431 and HeLa cells (half-maximal effective concentration (EC₅₀) values

were approximate 4–11 $\mu\text{g/mL}$ for A431 cells and 5–13 $\mu\text{g/mL}$ for HeLa cells, respectively; see Table 2). The EC_{50} value of Bz-PCL_{17,6}-PEG on A431 cells was lower than previously observed when mTHPC was loaded in micelles from slightly bigger benzyl-terminated Bz-PCL₂₃-PEG polymers (~35 $\mu\text{g/mL}$) under the same conditions [38]. A similar trend (i.e., increasing photocytotoxicity with decreasing polymer molecular weight) was observed before and attributed to faster intracellular degradation of smaller PCL-PEG block copolymers, and thus faster release of mTHPC after internalization by the cells [24]. It is worth noting that the observed EC_{50} values of these micellar mTHPC formulations on A431 and HeLa cells were slightly higher than free mTHPC (~1.5 $\mu\text{g/mL}$, Table 2), probably related to the less efficient cellular internalization of PEGylated micelles [53–55] or the relatively time-consuming degradation of polymers for release and activation of the PS [24].

Table 2. EC_{50} of free mTHPC and mTHPC-loaded in micelles (1 mg/mL polymer) on A431 and HeLa cells, obtained from the curves of Figure 5.

	EC_{50} ($\mu\text{g/mL}$)	
	A431	HeLa
Free mTHPC	1.6 \pm 0.1 [38]	1.2 [38]
Bz-PCL _{17,6} -PEG	10.7 \pm 0.5	13.0 \pm 0.8
P(CL _{13,5} -TMC-Bz _{3,7})-PEG	3.6 \pm 0.2	4.9 \pm 0.4
P(CL _{9,1} -TMC-Bz _{7,7})-PEG	8.6 \pm 0.3	9.4 \pm 0.6
P(CL _{4,8} -TMC-Bz _{9,2})-PEG	5.6 \pm 0.1	10.0 \pm 0.6

3.6. Pharmacokinetics and Biodistribution of mTHPC in its Free Form and Loaded in Cy7-Labeled Bz-PCL_{17,6}-PEG and P(CL_{9,1}-TMC-Bz_{7,7})-PEG Micelles in A431 Tumor-Bearing Mice

The circulation time and biodistribution of mTHPC-loaded micelles were studied using mice bearing human A431 tumor xenografts of 100–300 mm³. NIR fluorescence of Cy7-labeled micelles and mTHPC concentrations as measured in plasma and organ and tumor homogenates, thus addressing both polymer and photosensitizer contents of the samples. Micelles consisting of Bz-PCL_{17,6}-PEG and P(CL_{9,1}-TMC-Bz_{7,7})-PEG were chosen because both copolymers have comparable chain lengths of hydrophobic blocks (~18 units of either CL with the final unit capped with a benzyl group, or CL plus TMC-Bz) but different contents of aromatic units. Importantly, both micellar PS formulations showed similar phototoxicity on cells (Figure 5C,D) but markedly different release behaviors in vitro (Figure 3B).

The plasma concentrations were determined after intravenous administration of free mTHPC or Cy7-labeled micelles loaded with mTHPC into mice via the tail vein. As reported in our previous study [38], administration of free mTHPC (i.e., mTHPC dissolved in diluted Foscan solvent (ethanol/propylene glycol/PBS 20:30:50 *v/v/v*) inflicted side effects such as tachypnea, passiveness immediately post-injection, and loss of body weight (~1 g on average) within 24 h. However, none of the micellar mTHPC treated mice showed any (short term) side effects during or after their administration, suggesting micellar formulations at the injected polymer dose (~1 mg) are well tolerated for in vivo applications.

The analysis of Cy7 levels in plasma (Figure 6A) showed that the elimination rate of P(CL_{9,1}-TMC-Bz_{7,7})-PEG micelles was significantly slower as compared to that of Bz-PCL_{17,6}-PEG micelles (e.g., 55% vs 5% of the injected dose (ID) remaining in plasma after 1 h). Non-compartment analysis was used to determine the pharmacokinetic parameters of both micelles, including terminal half-life, area under the curve (AUC), and clearance. As shown in Table 3, Bz-PCL_{17,6}-PEG and P(CL_{9,1}-TMC-Bz_{7,7})-PEG micelles significantly differed in AUC values, and consequentially had large differences in distribution and clearance volumes. The differences in pharmacokinetic parameters primarily relate to the initial phase of the plasma curves (i.e., before 1 h); most likely they relate to differences in stability of the micelles, indicating more rapid dissociation of Bz-PCL_{17,6}-PEG micelles

into unimers as compared to P(CL_{9,1}-TMC-Bz_{7,7})-PEG micelles. This is most likely attributed to relatively stronger π - π stacking between the polymer chains in the latter micelles [30,56].

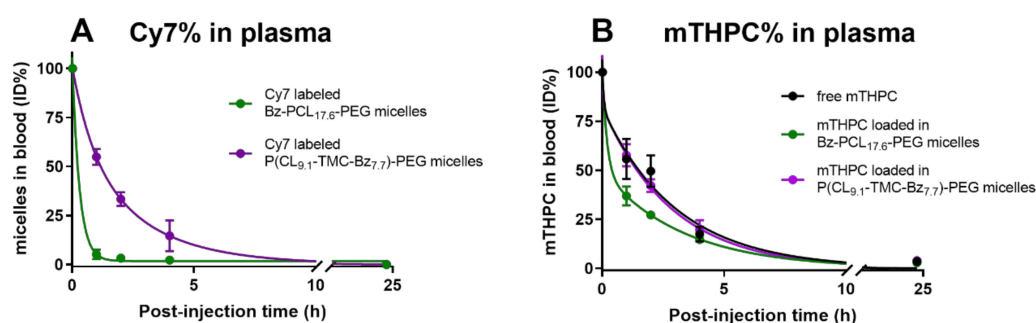


Figure 6. Plasma disappearance of free mTHPC (i.e., Foscan[®] formulation) and 0.6 wt% mTHPC-loaded Cy7-labeled micelles, showing Cy7 levels (A) and mTHPC levels (B) as % of injected doses (ID) upon tail vein administration in A431 tumor-bearing Balb/c mice (300 μ g mTHPC per kg bodyweight of the mouse, i.e., \sim 6 μ g mTHPC and \sim 1 mg polymer per mouse with injection volume of \sim 120 μ L). Data are presented as mean \pm SD, $n = 3$ –5.

Table 3. The half-life and the area under the curve (AUC) values of mTHPC in different formulations and the corresponding (Cy7-labeled) micelles.

Detection	Formulation	Half-life (h)		AUC (h*%)	Volume of Distribution (mL/kg)	Clearance (mL/kg/h)
		Phase α ^a	Phase β			
Cy7	Bz-PCL _{17,6} -PEG micelles	<0.3	-	72	306	81.4
	P(CL _{9,1} -TMC-Bz _{7,7})-PEG micelles	\sim 0.7	2.9	319	77	18.4
mTHPC	Free mTHPC	\leq 0.5	2.1	442	120	13.2
	mTHPC in Bz-PCL _{17,6} -PEG micelles	\leq 0.5	2.5	350	180	16.7
	mTHPC in P(CL _{9,1} -TMC-Bz _{7,7})-PEG micelles	\leq 0.5	2.0	464	120	12.6

^a Initial phase half-lives ($t_{1/2-\alpha}$) were estimated from plasma disappearance rates during the first hour after administration, while half-lives of the terminal phase ($t_{1/2-\beta}$) were calculated from non-compartmental analysis. Distribution volumes and clearances were calculated assuming a standard blood volume of 58.5 mL/kg [24].

Figure 6B shows the plasma concentrations of mTHPC after administration of either free mTHPC or the micellar formulations. It is clear that free mTHPC and mTHPC loaded in micelles displayed comparable mTHPC levels and showed similar decay profiles in the circulation (Figure 6B). A rapid initial elimination was observed, for which half-lives ($t_{1/2-\alpha}$) of \sim 0.5 h or less were estimated. Non-compartmental analysis of the mTHPC curves provided terminal half-lives ($t_{1/2-\beta}$), AUCs, and derived pharmacokinetic parameters, such as distribution volumes and clearance. It can be concluded from the results presented in Table 3 (bottom part) that those pharmacokinetic parameters were comparable between both free mTHPC and micellar mTHPC formulations. In addition, significant differences of pharmacokinetic parameters were observed between both Bz-PCL_{17,6}-PEG micelles and the loaded mTHPC, indicating that PS and polymer dissociated rapidly upon their injection into the circulation. On the other hand, for P(CL_{9,1}-TMC-Bz_{7,7})-PEG micellar formulation, pharmacokinetic parameters of mTHPC (Table 3, bottom part) were tightly associated with those derived from Cy7 analysis (Table 3, top part). However, due to coincidentally similar data observed for free mTHPC and Cy7, it is difficult to conclude based on these parameters whether mTHPC was released from P(CL_{9,1}-TMC-Bz_{7,7})-PEG micelles or retained in the micelles. However, the in vitro release study in human plasma (Figure 3B, purple line and Figure 4) suggests that premature release of mTHPC from micelles most likely also occurred in the circulation for these micelles. Similarly, it was reported that paclitaxel loaded in thermosensitive micelles containing aromatic HPMAM-Bz units in the hydrophobic blocks exhibited a similar pharmacokinetic profile as when loaded in micelles without

aromatic groups and as compared to free paclitaxel, despite the significantly improved in vitro stability and drug retention by π - π stacking [30,56]. Additionally, paclitaxel loaded in thermosensitive HPMAm-lactate-based micelles also showed the same pharmacokinetic data as the drug in its free form [57]. In addition, premature cargo release was also observed previously in various liposomal mTHPC formulations and other mTHPC-loaded micelles [24,58]. This release can be attributed to the high binding affinity of mTHPC with plasma (lipo)proteins, leading to mTHPC redistribution from intact micelles to these plasma components [59–61]. It is noted that the relatively long circulation time of (released) mTHPC in the β phase is probably due to released mTHPC that subsequently binds to lipoproteins, which can act as endogenous carriers for mTHPC [62,63].

Tumors and organs were excised from mice that were sacrificed at 4 and 24 h after i.v. injection and Cy7-labeled micelles deposited in these tissues were visualized using 2D fluorescence reflectance imaging (FRI) and subsequently quantified by fluorescence intensity. It is noted that before taking out the organs, cervical dislocation followed by a cardiac puncture was performed for all mice, through which a substantial volume of blood was drawn from the animal in order to minimize the background signal from residual blood in the tissues. As shown in Figure 7, ex vivo images indicate that both Bz-PCL_{17.6}-PEG and P(CL_{9.1}-TMC-Bz_{7.7})-PEG micelles were found to primarily accumulate in liver, followed by kidneys and spleen. Different organ distribution profiles were observed for the two micellar formulations. As an explanation, Bz-PCL_{17.6}-PEG micelles accumulated in liver and kidneys at 4 h and while the accumulation in liver decayed, kidney accumulation persisted upon 24 h after administration. Accumulation of P(CL_{9.1}-TMC-Bz_{7.7})-PEG micelles in the kidneys was less pronounced and these micelles showed prolonged residence up to 24 h in the liver, and to a lesser extent in the spleen. In line with the imaging results, the quantified fluorescence intensities (Figure 8) show that the prominent liver accumulation of both micelles (Figure 8A) was observed to be ~15% ID/g at 4 h, in line with previous reports [30,64], most likely due to their clearance by the mononuclear phagocytic system (MPS) [65–67]. However, 24 h post-injection, Bz-PCL_{17.6}-PEG micelles decreased significantly to approximately 5% ID/g liver, while P(CL_{9.1}-TMC-Bz_{7.7})-PEG micelles remained at similar levels in the liver as observed at 4 h. Additionally, the residence of the P(CL_{9.1}-TMC-Bz_{7.7})-PEG micelles in the spleen was significantly longer than Bz-PCL_{17.6}-PEG micelles (4.6% vs 1.4% ID/g after 24 h, Figure 8D). These results suggest better stability of the P(CL_{9.1}-TMC-Bz_{7.7})-PEG micelles than the micelles from Bz-terminated polymers, most likely due to strong π - π stacking resulting from the multiple Bz groups per polymer chain in the micelles of the former. Cy7 levels from Bz-PCL_{17.6}-PEG and P(CL_{9.1}-TMC-Bz_{7.7})-PEG micelles could be detected in kidneys with ~6% and ~4% ID/g (Figure 8B) at 4 h, respectively, which decreased slightly at 24 h. The observed kidney accumulation was most likely due to dissociation of Cy7-labeled unimers from the micelles, which have a molecular size below the threshold of glomerular filtration [65].

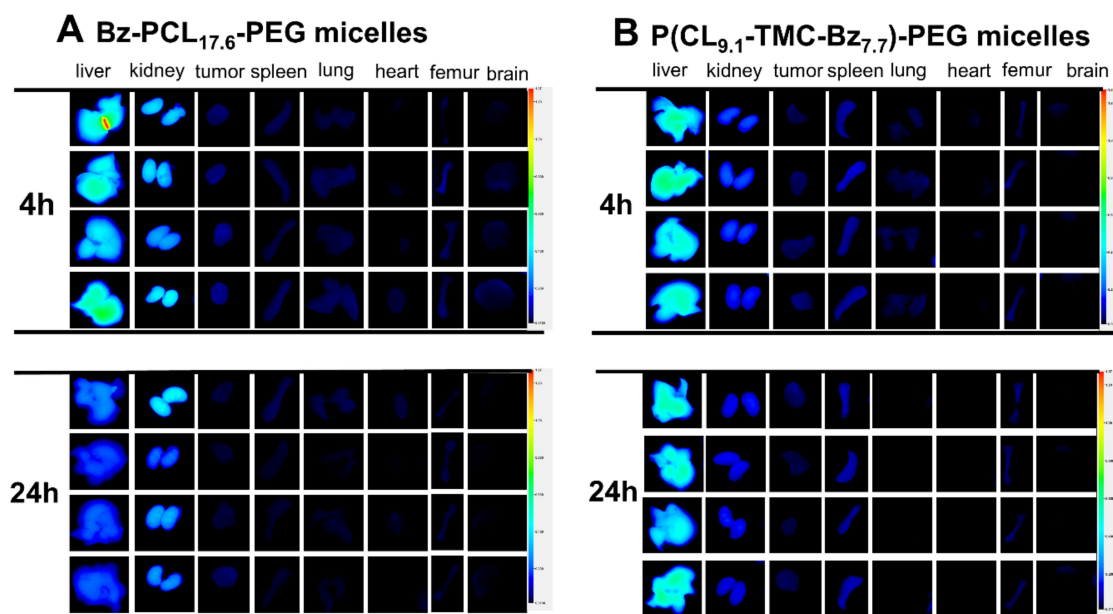


Figure 7. Ex vivo fluorescence reflectance imaging (FRI) analysis of the accumulation of the Cy7-labeled Bz-PCL_{17.6}-PEG (A) and P(CL_{9.1}-TMC-Bz_{7.7})-PEG (B) micelles in tumors and healthy organs after 4 and 24 h administration. Images, obtained at λ_{em} 820 nm with λ_{ex} 785 nm are from 4 different mice at each timepoint ($n = 4$).

Interestingly, although no micelles were detected in the circulation after 24 h (Figure 6), accumulation of P(CL_{9.1}-TMC-Bz_{7.7})-PEG micelles in tumors increased from 0.6 % ID/g at 4 h to approximate 1% ID/g at 24 h (Figure 8C). In contrast, no tumor accumulation of Bz-PCL_{17.6}-PEG micelles was found at 24 h. This suggests that after 4 h, the remaining P(CL_{9.1}-TMC-Bz_{7.7})-PEG micelles in the circulation (15 % ID, Figure 6) were (at least partly) intact and progressively accumulated in tumors via overtime EPR effect. In addition, P(CL_{9.1}-TMC-Bz_{7.7})-PEG micelles accumulated in significantly higher amounts in the femur at 4 and 24 h than Bz-PCL_{17.6}-PEG micelles (Figure 8G). This also indicates the higher amount of intact micelles present in the circulation, since it was previously reported that relatively small nanoparticles (generally below 60 nm) tend to accumulate in MPS-enriched bone marrow [68,69].

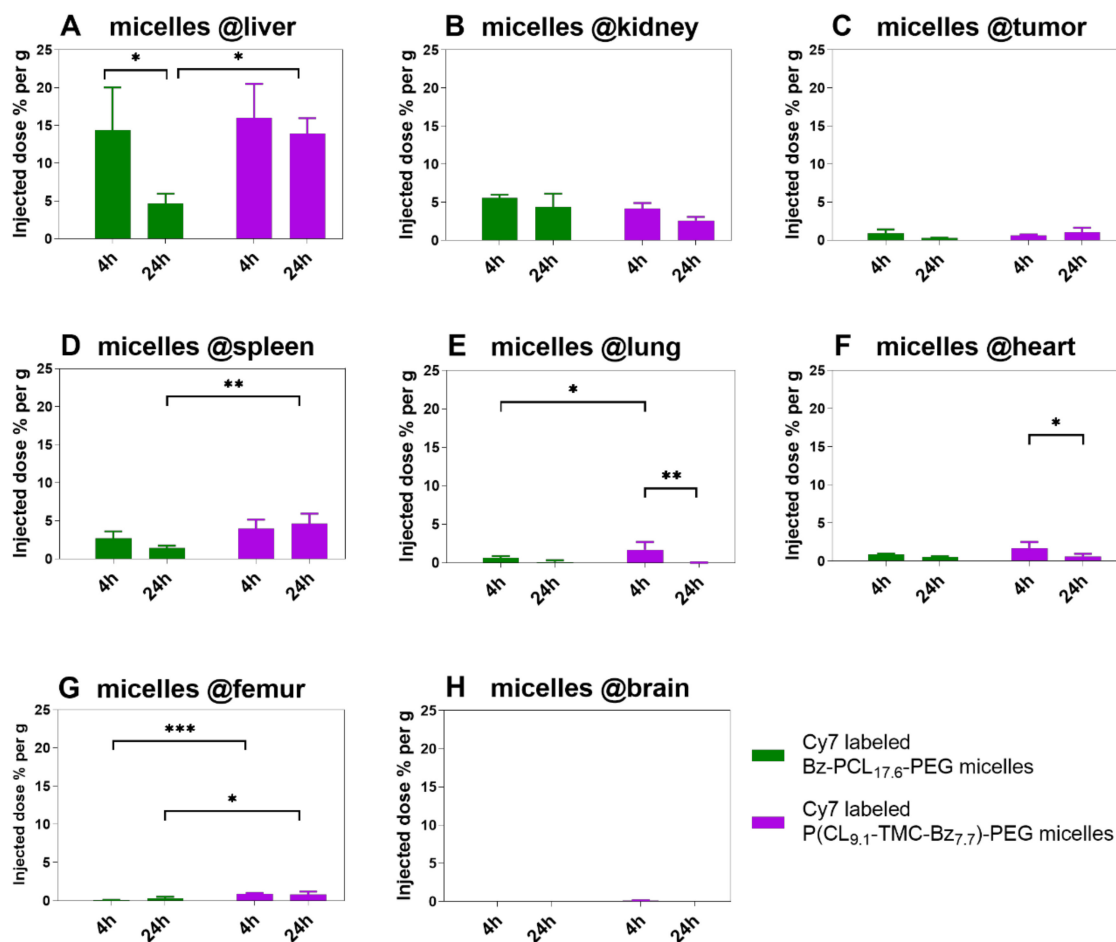


Figure 8. Biodistribution of Cy7-labeled micelles in tumor and main organs of mice after 4 and 24 h administration, (A) liver, (B) kidney, (C) tumor, (D) spleen, (E) lung, (F) heart, (G) femur, (H) brain. Data are indicated as the percentage of the injected Cy7 dose (%ID) present per gram of tumor or organ ($n = 3-5$). * $p < 0.05$, ** $p < 0.01$, *** $p < 0.001$.

To study a possible correlation of biodistribution between mTHPC and micelles, Figure 9 displays the biodistribution in tumors and a panel of organs of mTHPC that was injected in free form and using Bz-PCL_{17.6}-PEG or P(CL_{9.1}-TMC-Bz_{7.7})-PEG formulations. The first conclusion is that the biodistribution of micellar mTHPC was similar to that of free mTHPC. The highest mTHPC levels were seen in liver and spleen, followed by lungs (Figure 9A,D,E). These are all tissues containing reticuloendothelial cells with a rich MPS, which are known to preferentially accumulate photosensitizers [8,70–72]. The accumulation of mTHPC in the liver at 4 h was similar to the accumulation of polymers in the liver (i.e., ~15% ID per gram), which then decreased significantly to about 5% ID/g at 24 h (Figure 9A). Higher accumulation of mTHPC in lungs was observed after 4 h than after 24 h (Figure 9E), most likely due to the blood fraction (containing mTHPC) after 4 h present in the excised lungs of non-perfused mice. However, in spleen and lungs, higher accumulation of mTHPC (~8–15% ID/g, Figure 9D,E, green and purple columns) was detected than that of the corresponding host micelles ($\leq 5\%$ ID/g, Figure 8D,E). The values of mTHPC accumulation were consistent with those reported for mTHPC when dosed using different liposomal formulations [58,72,73]. It is noted that although similar mTHPC content was detected per gram for the three organs, the total mTHPC accumulation in liver was significantly higher than that in spleen and lungs (e.g., ~15% ID per liver vs. ~1% ID per spleen or lung at 4 h; Figure S12A,D,E of Supplementary Materials) due to the high weights of liver samples (~1 g on average). Apart from liver, spleen, and lungs, regardless of the timepoints, similar amounts of mTHPC (~2–3% ID/g) were accumulated in tumor, kidney,

heart, and femur (Figure 9B,C,F,G), suggesting unspecific biodistribution of mTHPC. Accumulated mTHPC levels resulting from being loaded in Bz-PCL_{17.6}-PEG and P(CL_{9.1}-TMC-Bz_{7.7})-PEG micelles in these organs and tissues (Figure 9C,F,G, green and purple columns) were higher as compared to the corresponding host micelles (<1%) (Figure 8C,F,G), except those in the kidney (Figures 8B and 9B). This loose association of the distribution pattern between mTHPC and the host micelles confirmed the fast release of mTHPC from both micelles. It is noted that neither the PS nor the micelles showed disposition in the brain (Figures 8H and 9H), which is a well-perfused organ; thus, the background signal from residual blood in the tissues appears minimal.

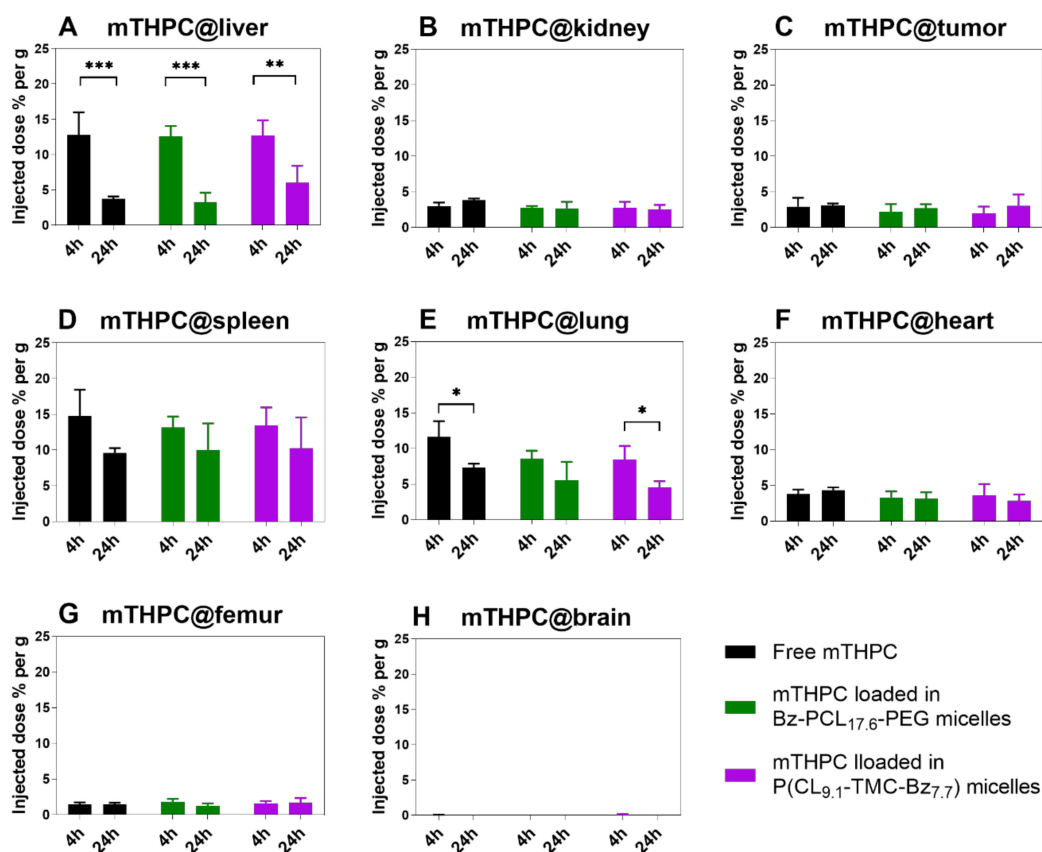


Figure 9. Biodistribution of free mTHPC and mTHPC loaded in micelles in tumors and main organs of mice after 4 and 24 h administration at mTHPC dose of 0.3 mg/kg, (A) liver, (B) kidney, (C) tumor, (D) spleen, (E) lung, (F) heart, (G) femur, (H) brain. Data are indicated as the percentage of the injected mTHPC dose (%ID) present per gram of tumor or organ ($n = 3-5$). * $p < 0.05$, ** $p < 0.01$, *** $p < 0.001$.

4. Conclusions

In the present study, we showed that i.v. injected micelles containing multiple pendant aromatic groups (i.e., TMC-Bz monomers) in the hydrophobic blocks of the PCL-PEG-based block copolymers displayed longer circulation times in mice than micelles with a single terminal aromatic group, and that incorporating the pendant aromatic groups improved retention of the photosensitizer mTHPC in human plasma in vitro. Despite those promising features, similar biodistribution of micellar mTHPC as compared to free mTHPC—and importantly, unequal biodistribution patterns of mTHPC and the host micelles—indicated premature release of mTHPC from these micelles in vivo. Our study emphasizes the necessity to investigate the in vivo behavior, particularly biodistribution, of both the micellar carrier and the incorporated cargo, as such data can provide important information about the fate of PS-loaded nanocarriers. Our study shows that additional measures beyond π - π stacking are needed to stably incorporate mTHPC in the micelles in order to benefit from them as carriers that are able to deliver the payload in pathological tissue by passive or active targeting.

Supplementary Materials: The following are available online at <http://www.mdpi.com/1999-4923/12/4/338/s1>, Scheme S1: Synthesis and Cy7 labeling of P(CL₁₈-TTC_{7.5})-PEG, Figure S1: DSC thermograms of TMC-Bz and its precursor, Figure S2: ¹H/¹³C NMR spectra of TMC-Bz and its precursor, Figure S3: ¹H NMR spectrum of P(CL-TMC-Bz)-PEG, Figure S4: ¹H NMR spectrum of P(TMC-Bz)-PEG, Figure S5: ¹H NMR spectrum of PCL-PEG, Figure S6: ¹H NMR spectrum of Bz-PCL-PEG, Figure S7: DSC thermograms of P(CL_{9,1}-TMC-Bz_{7,7})-PEG (Entry 7, Table 1) and PCL_{17,6}-PEG (Entry 5, Table 1), Figure S8: melting enthalpies of PEG corrected for the weight fraction of PEG in the block copolymers, and glass transition temperatures (measured and predicted based on FOX equation) of P(CL-TMC-Bz)-PEG copolymers with random CL and TMC-Bz sequence, Figure S9: DLS data of PCL₉-PEG micelles in PBS, Figure S10: Fluorescence intensity of mTHPC-loaded micelles as a function of time at 37 °C in PBS, Figure S11: Cytotoxicity of empty micelles on A431 and HeLa cells, Figure S12: Biodistribution of free mTHPC and mTHPC loaded in micelles.

Author Contributions: Conceptualization, C.F.v.N.; funding acquisition, Y.L. and C.F.v.N.; investigation, Y.L., M.H.A.M.F., B.L., N.C.H.v.K., and R.F.M.M.-B.; methodology, R.J.K.; supervision, S.O., W.E.H., and C.F.v.N. All authors have read and agreed to the published version of the manuscript.

Funding: Y. Liu is supported by a PhD scholarship from China Scholarship Council (CSC) (File no. 201506220178).

Conflicts of Interest: The authors declare no conflict of interest.

References

1. Van Straten, D.; Mashayekhi, V.; de Bruijn, H.S.; Oliveira, S.; Robinson, D.J. Oncologic photodynamic therapy: Basic principles, current clinical status and future directions. *Cancers* **2017**, *9*, 19. [[CrossRef](#)] [[PubMed](#)]
2. Yakavets, I.; Millard, M.; Zorin, V.; Lassalle, H.P.; Bezdetnaya, L. Current state of the nanoscale delivery systems for temoporfin-based photodynamic therapy: Advanced delivery strategies. *J. Control. Release* **2019**, *304*, 268–287. [[CrossRef](#)] [[PubMed](#)]
3. Agostinis, P.; Berg, K.; Cengel, K.A.; Foster, T.H.; Girotti, A.W.; Gollnick, S.O.; Hahn, S.M.; Hamblin, M.R.; Juzeniene, A.; Kessel, D.; et al. Photodynamic therapy of cancer: An update. *CA Cancer J. Clin.* **2011**, *61*, 250–281. [[CrossRef](#)] [[PubMed](#)]
4. Hernández, I.; Yu, Y.; Ossendorp, F.; Korbelik, M.; Oliveira, S. Preclinical and clinical evidence of immune responses triggered in oncologic photodynamic therapy: Clinical recommendations. *J. Clin. Med.* **2020**, *9*, 1–25.
5. Meulemans, J.; Delaere, P.; Vander Poorten, V. Photodynamic therapy in head and neck cancer: Indications, outcomes, and future prospects. *Curr. Opin. Otolaryngol. Head Neck Surg.* **2019**, *27*, 136–141. [[CrossRef](#)]
6. Van Driel, P.; Boonstra, M.C.; Slooter, M.D.; Heukers, R.; Stammes, M.A.; Snoeks, T.J.A.; de Bruijn, H.S.; van Diest, P.J.; Vahrmeijer, A.L.; van Bergen En Henegouwen, P.M.P.; et al. EGFR targeted nanobody-photosensitizer conjugates for photodynamic therapy in a pre-clinical model of head and neck cancer. *J. Control. Release* **2016**, *229*, 93–105. [[CrossRef](#)]
7. Hopper, C. Photodynamic therapy: A clinical reality in the treatment of cancer. *Lancet Oncol.* **2000**, *1*, 212–219. [[CrossRef](#)]
8. Bovis, M.J.; Woodhams, J.H.; Loizidou, M.; Scheglmann, D.; Bown, S.G.; MacRobert, A.J. Improved in vivo delivery of m-THPC via pegylated liposomes for use in photodynamic therapy. *J. Control. Release* **2012**, *157*, 196–205. [[CrossRef](#)]
9. Kwiatkowski, S.; Knap, B.; Przystupski, D.; Saczko, J.; Kedzierska, E.; Knap-Czop, K.; Kotlinska, J.; Michel, O.; Kotowski, K.; Kulbacka, J. Photodynamic therapy—Mechanisms, photosensitizers and combinations. *Biomed. Pharmacother.* **2018**, *106*, 1098–1107. [[CrossRef](#)]
10. Redmond, R.W.; Land, E.J.; Truscott, T.G. Aggregation effects on the photophysical properties of porphyrins in relation to mechanisms involved in photodynamic therapy. *Adv. Exp. Med. Biol.* **1985**, *193*, 293–302.
11. Triesscheijn, M.; Ruevekamp, M.; Out, R.; Van Berkel, T.J.; Schellens, J.; Baas, P.; Stewart, F.A. The pharmacokinetic behavior of the photosensitizer meso-tetra-hydroxyphenyl-chlorin in mice and men. *Cancer Chemother. Pharmacol.* **2007**, *60*, 113–122. [[CrossRef](#)] [[PubMed](#)]
12. Van Nostrum, C.F. Polymeric micelles to deliver photosensitizers for photodynamic therapy. *Adv. Drug Deliv. Rev.* **2004**, *56*, 9–16. [[CrossRef](#)] [[PubMed](#)]

13. Deng, C.; Jiang, Y.; Cheng, R.; Meng, F.; Zhong, Z. Biodegradable polymeric micelles for targeted and controlled anticancer drug delivery: Promises, progress and prospects. *Nano Today* **2012**, *7*, 467–480. [[CrossRef](#)]
14. Varela-Moreira, A.; Shi, Y.; Fens, M.H.A.M.; Lammers, T.; Hennink, W.E.; Schiffelers, R.M. Clinical application of polymeric micelles for the treatment of cancer. *Mater. Chem. Front.* **2017**, *1*, 1485–1501. [[CrossRef](#)]
15. Cabral, H.; Kataoka, K. Progress of drug-loaded polymeric micelles into clinical studies. *J. Control. Release* **2014**, *190*, 465–476. [[CrossRef](#)]
16. Houdaihed, L.; Evans, J.C.; Allen, C. Overcoming the road blocks: Advancement of block copolymer micelles for cancer therapy in the clinic. *Mol. Pharm.* **2017**, *14*, 2503–2517. [[CrossRef](#)]
17. Dos Santos, N.; Allen, C.; Doppen, A.M.; Anantha, M.; Cox, K.A.; Gallagher, R.C.; Karlsson, G.; Edwards, K.; Kenner, G.; Samuels, L.; et al. Influence of poly(ethylene glycol) grafting density and polymer length on liposomes: Relating plasma circulation lifetimes to protein binding. *Biochim. Biophys. Acta* **2007**, *1768*, 1367–1377. [[CrossRef](#)]
18. Klibanov, A.L.; Maruyama, K.; Torchilin, V.P.; Huang, L. Amphipathic polyethyleneglycols effectively prolong the circulation time of liposomes. *FEBS Lett.* **1990**, *268*, 235–237. [[CrossRef](#)]
19. Torchilin, V.P. Recent advances with liposomes as pharmaceutical carriers. *Nat. Rev. Drug Discov.* **2005**, *4*, 145–160. [[CrossRef](#)]
20. Tan, C.; Wang, Y.; Fan, W. Exploring polymeric micelles for improved delivery of anticancer agents: Recent developments in preclinical studies. *Pharmaceutics* **2013**, *5*, 201–219. [[CrossRef](#)]
21. Maeda, H. Toward a full understanding of the EPR effect in primary and metastatic tumors as well as issues related to its heterogeneity. *Adv. Drug Deliv. Rev.* **2015**, *91*, 3–6. [[CrossRef](#)] [[PubMed](#)]
22. Maeda, H.; Wu, J.; Sawa, T.; Matsumura, Y.; Hori, K. Tumor vascular permeability and the EPR effect in macromolecular therapeutics: A review. *J. Control. Release* **2000**, *65*, 271–284. [[CrossRef](#)]
23. Hofman, J.W.; Carstens, M.G.; van Zeeland, F.; Helwig, C.; Flesch, F.M.; Hennink, W.E.; van Nostrum, C.F. Photocytotoxicity of mTHPC (temoporfin) loaded polymeric micelles mediated by lipase catalyzed degradation. *Pharm. Res.* **2008**, *25*, 2065–2073. [[CrossRef](#)]
24. Wennink, J.W.H.; Liu, Y.; Makinen, P.I.; Setaro, F.; de la Escosura, A.; Bourajaj, M.; Lappalainen, J.P.; Holappa, L.P.; van den Dikkenberg, J.B.; Al Fartousi, M.; et al. Macrophage selective photodynamic therapy by meta-tetra(hydroxyphenyl)chlorin loaded polymeric micelles: A possible treatment for cardiovascular diseases. *Eur. J. Pharm. Sci.* **2017**, *107*, 112–125. [[CrossRef](#)] [[PubMed](#)]
25. Gong, J.; Chen, M.; Zheng, Y.; Wang, S.; Wang, Y. Polymeric micelles drug delivery system in oncology. *J. Control. Release* **2012**, *159*, 312–323. [[CrossRef](#)] [[PubMed](#)]
26. Sheridan, C. Proof of concept for next-generation nanoparticle drugs in humans. *Nat. Biotechnol.* **2012**, *30*, 471–473. [[CrossRef](#)]
27. Wang, A.Z.; Langer, R.; Farokhzad, O.C. Nanoparticle delivery of cancer drugs. *Annu. Rev. Med.* **2012**, *63*, 185–198. [[CrossRef](#)]
28. Talelli, M.; Barz, M.; Rijcken, C.J.F.; Kiessling, F.; Hennink, W.E.; Lammers, T. Core-crosslinked polymeric micelles: Principles, preparation, biomedical applications and clinical translation. *Nano Today* **2015**, *10*, 93–117. [[CrossRef](#)]
29. Hamaguchi, T.; Matsumura, Y.; Suzuki, M.; Shimizu, K.; Goda, R.; Nakamura, I.; Nakatomi, I.; Yokoyama, M.; Kataoka, K.; Kakizoe, T. NK105, a paclitaxel-incorporating micellar nanoparticle formulation, can extend in vivo antitumour activity and reduce the neurotoxicity of paclitaxel. *Br. J. Cancer* **2005**, *92*, 1240–1246. [[CrossRef](#)]
30. Shi, Y.; van der Meel, R.; Theek, B.; Oude Blenke, E.; Pieters, E.H.; Fens, M.H.; Ehling, J.; Schiffelers, R.M.; Storm, G.; van Nostrum, C.F.; et al. Complete regression of xenograft tumors upon targeted delivery of paclitaxel via π - π stacking stabilized polymeric micelles. *ACS Nano* **2015**, *9*, 3740–3752. [[CrossRef](#)]
31. Shi, Y.; Lammers, T.; Storm, G.; Hennink, W.E. Physico-chemical strategies to enhance stability and drug retention of polymeric micelles for tumor-targeted drug delivery. *Macromol. Biosci.* **2017**, *17*, 1–11. [[CrossRef](#)] [[PubMed](#)]
32. Zhuang, W.; Wang, Y.; Cui, P.; Xing, L.; Lee, J.; Kim, D.; Jiang, H.; Oh, Y. Applications of π - π stacking interactions in the design of drug-delivery systems. *J. Control. Release* **2019**, *294*, 311–326. [[CrossRef](#)] [[PubMed](#)]

33. Shi, Y.; Elkhazab, A.; Yengej, F.A.; van den Dikkenberg, J.; Hennink, W.E.; van Nostrum, C.F. π - π stacking induced enhanced molecular solubilization, singlet oxygen production, and retention of a photosensitizer loaded in thermosensitive polymeric micelles. *Adv. Healthc. Mater.* **2014**, *3*, 2023–2031. [[CrossRef](#)] [[PubMed](#)]
34. Pratt, R.C.; Nederberg, F.; Waymouth, R.M.; Hedrick, J.L. Tagging alcohols with cyclic carbonate: A versatile equivalent of (meth)acrylate for ring-opening polymerization. *Chem. Commun.* **2008**, 114–116. [[CrossRef](#)]
35. Couffin, A.; Delcroix, D.; Martín-Vaca, B.; Bourissou, D.; Navarro, C. Mild and efficient preparation of block and gradient copolymers by methanesulfonic acid catalyzed ring-opening polymerization of caprolactone and trimethylene carbonate. *Macromolecules* **2013**, *46*, 4354–4360. [[CrossRef](#)]
36. Delcroix, D.; Martín-Vaca, B.; Bourissou, D.; Navarro, C. Ring-opening polymerization of trimethylene carbonate catalyzed by methanesulfonic acid: Activated monomer versus active chain end mechanisms. *Macromolecules* **2010**, *43*, 8828–8835. [[CrossRef](#)]
37. Carstens, M.G.; van Nostrum, C.F.; Ramzi, A.; Meeldijk, J.D.; Verrijck, R.; de Leede, L.L.; Crommelin, D.J.; Hennink, W.E. Poly(ethylene glycol)-oligolactates with monodisperse hydrophobic blocks: Preparation, characterization, and behavior in water. *Langmuir* **2005**, *21*, 11446–11454. [[CrossRef](#)]
38. Liu, Y.; Scrivano, L.; Peterson, J.D.; Fens, M.H.A.M.; Hernández, I.B.; Mesquita, B.; Toraño, J.S.; Hennink, W.E.; Nostrum, C.F.; Oliveira, S. EGFR targeted nanobody functionalized polymeric micelles loaded with mTHPC for selective photodynamic therapy. *Mol. Pharm.* **2020**, *17*, 1276–1292. [[CrossRef](#)]
39. Bagheri, M.; Bresseleers, J.; Varela-Moreira, A.; Sandre, O.; Meeuwissen, S.A.; Schiffelers, R.M.; Metselaar, J.M.; van Nostrum, C.F.; van Hest, J.C.M.; Hennink, W.E. Effect of formulation and processing parameters on the size of mPEG-*b*-p(HPMA-Bz) polymeric micelles. *Langmuir* **2018**, *34*, 15495–15506. [[CrossRef](#)]
40. Zhang, Y.; Huo, M.; Zhou, J.; Xie, S. PKSolver: An add-in program for pharmacokinetic and pharmacodynamic data analysis in Microsoft Excel. *Comput. Methods Programs Biomed.* **2010**, *99*, 306–314. [[CrossRef](#)]
41. Schindler, A.; Hibionada, Y.M.; Pitt, C.G. Aliphatic polyesters. III. Molecular weight and molecular weight distribution in alcohol-initiated polymerizations of ϵ -caprolactone. *J. Polym. Sci. Polym. Chem. Ed.* **1982**, *20*, 319–326. [[CrossRef](#)]
42. Pêgo, A.P.; Zhong, Z.; Dijkstra, P.J.; Grijpma, D.W.; Feijen, J. Influence of catalyst and polymerization conditions on the properties of 1,3-trimethylene carbonate and ϵ -caprolactone copolymers. *Macromol. Chem. Phys.* **2003**, *204*, 747–754. [[CrossRef](#)]
43. Loontjens, C.A.M.; Vermonden, T.; Leemhuis, M.; van Steenbergen, M.J.; van Nostrum, C.F.; Hennink, W.E. Synthesis and characterization of random and triblock copolymers of ϵ -caprolactone and (Benzylated)hydroxymethyl glycolide. *Macromolecules* **2007**, *40*, 7208–7216. [[CrossRef](#)]
44. Ling, J.; Zhu, W.; Shen, Z. Controlling ring-opening copolymerization of ϵ -caprolactone with trimethylene carbonate by scandium Tris(2,6-di-*tert*-butyl-4-methylphenolate). *Macromolecules* **2004**, *37*, 758–763. [[CrossRef](#)]
45. Carstens, M.G.; Bevernage, J.J.L.; van Nostrum, C.F.; van Steenbergen, M.J.; Flesch, F.M.; Verrijck, R.; de Leede, L.G.J.; Crommelin, D.J.A.; Hennink, W.E. Small oligomeric micelles based on end group modified mPEG-oligocaprolactone with monodisperse hydrophobic blocks. *Macromolecules* **2007**, *40*, 116–122. [[CrossRef](#)]
46. Cabral, H.; Matsumoto, Y.; Mizuno, K.; Chen, Q.; Murakami, M.; Kimura, M.; Terada, Y.; Kano, M.R.; Miyazono, K.; Uesaka, M.; et al. Accumulation of sub-100 nm polymeric micelles in poorly permeable tumours depends on size. *Nat. Nanotechnol.* **2011**, *6*, 815–823. [[CrossRef](#)] [[PubMed](#)]
47. Danhier, F.; Feron, O.; Preat, V. To exploit the tumor microenvironment: Passive and active tumor targeting of nanocarriers for anti-cancer drug delivery. *J. Control. Release* **2010**, *148*, 135–146. [[CrossRef](#)]
48. Jain, R.K.; Stylianopoulos, T. Delivering nanomedicine to solid tumors. *Nat. Rev. Clin. Oncol.* **2010**, *7*, 653–664. [[CrossRef](#)]
49. Rijcken, C.J.; Hofman, J.W.; van Zeeland, F.; Hennink, W.E.; van Nostrum, C.F. Photosensitizer-loaded biodegradable polymeric micelles: Preparation, characterisation and in vitro PDT efficacy. *J. Control. Release* **2007**, *124*, 144–153. [[CrossRef](#)]
50. Gaio, E.; Scheglmann, D.; Reddi, E.; Moret, F. Uptake and photo-toxicity of Foscan[®], Foslip[®] and Fospeg[®] in multicellular tumor spheroids. *J. Photochem. Photobiol. B* **2016**, *161*, 244–252. [[CrossRef](#)]
51. Gyenge, E.B.; Hiestand, S.; Graefe, S.; Walt, H.; Maake, C. Cellular and molecular effects of the liposomal mTHPC derivative Foslipos in prostate carcinoma cells in vitro. *Photodiagn. Photodyn. Ther.* **2011**, *8*, 86–96. [[CrossRef](#)]

52. Kiesslich, T.; Berlanda, J.; Plaetzer, K.; Krammer, B.; Berr, F. Comparative characterization of the efficiency and cellular pharmacokinetics of Foscan- and Foslip-based photodynamic treatment in human biliary tract cancer cell lines. *Photochem. Photobiol. Sci.* **2007**, *6*, 619–627. [[CrossRef](#)] [[PubMed](#)]
53. Chen, Y.; Tezcan, O.; Li, D.; Beztsinna, N.; Lou, B.; Etrych, T.; Ulbrich, K.; Metselaar, J.M.; Lammers, T.; Hennink, W.E. Overcoming multidrug resistance using folate receptor-targeted and pH-responsive polymeric nanogels containing covalently entrapped doxorubicin. *Nanoscale* **2017**, *9*, 10404–10419. [[CrossRef](#)] [[PubMed](#)]
54. Terashima, T.; Sugita, T.; Fukae, K.; Sawamoto, M. Synthesis and single-chain folding of amphiphilic random copolymers in water. *Macromolecules* **2014**, *47*, 589–600. [[CrossRef](#)]
55. Xie, J.; Xu, C.; Kohler, N.; Hou, Y.; Sun, S. Controlled PEGylation of monodisperse Fe₃O₄ nanoparticles for reduced non-specific uptake by macrophage cells. *Adv. Mater.* **2007**, *19*, 3163–3166. [[CrossRef](#)]
56. Shi, Y.; van Steenberg, M.J.; Teunissen, E.A.; Novo, L.; Gradmann, S.; Baldus, M.; van Nostrum, C.F.; Hennink, W.E. π - π stacking increases the stability and loading capacity of thermosensitive polymeric micelles for chemotherapeutic drugs. *Biomacromolecules* **2013**, *14*, 1826–1837. [[CrossRef](#)]
57. Soga, O. Biodegradable Thermosensitive Polymers: Synthesis, Characterization and Drug Delivery Applications. Ph.D. Thesis, Utrecht University, Utrecht, The Netherlands, 2006; pp. 87–102.
58. Decker, C.; Schubert, H.; May, S.; Fahr, A. Pharmacokinetics of temoporfin-loaded liposome formulations: Correlation of liposome and temoporfin blood concentration. *J. Control. Release* **2013**, *166*, 277–285. [[CrossRef](#)]
59. Polo, L.; Valduga, G.; Jori, G.; Reddi, E. Low-density lipoprotein receptors in the uptake of tumour photosensitizers by human and rat transformed fibroblasts. *Int. J. Biochem. Cell Biol.* **2002**, *34*, 10–23. [[CrossRef](#)]
60. Chowdhary, R.; Sharif, I.; Chansarkar, N.; Dolphin, D.; Delaney, S.; Meadows, H. Correlation of photosensitizer delivery to lipoproteins and efficacy in tumor and arthritis mouse models; comparison of lipid-based and Pluronic P123 formulations. *J. Pharm. Pharm. Sci.* **2003**, *6*, 198–204.
61. Sasnouski, S.; Zorin, V.; Khludeyev, I.; D’Hallewin, M.A.; Guillemin, F.; Bezdetsnaya, L. Investigation of Foscan interactions with plasma proteins. *Biochim. Biophys. Acta* **2005**, *1725*, 394–402. [[CrossRef](#)]
62. Michael-Titus, A.T.; Whelpton, R.; Yaqub, Z. Binding of temoporfin to the lipoprotein fractions of human serum. *Br. J. Clin. Pharmacol.* **1995**, *40*, 594–597. [[CrossRef](#)] [[PubMed](#)]
63. Reshetov, V.; Zorin, V.; Siupa, A.; D’Hallewin, M.A.; Guillemin, F.; Bezdetsnaya, L. Interaction of liposomal formulations of meta-tetra(hydroxyphenyl)chlorin (temoporfin) with serum proteins: Protein binding and liposome destruction. *Photochem. Photobiol.* **2012**, *88*, 1256–1264. [[CrossRef](#)] [[PubMed](#)]
64. Shi, Y.; Kunjachan, S.; Wu, Z.; Gremse, F.; Moeckel, D.; van Zandvoort, M.; Kiessling, F.; Storm, G.; van Nostrum, C.F.; Hennink, W.E.; et al. Fluorophore labeling of core-crosslinked polymeric micelles for multimodal in vivo and ex vivo optical imaging. *Nanomedicine* **2015**, *10*, 1111–1125. [[CrossRef](#)]
65. Noguchi, Y.; Wu, J.; Duncan, R.; Strohal, J.; Ulbrich, K.; Akaike, T.; Maeda, H. Early phase tumor accumulation of macromolecules: A great difference in clearance rate between tumor and normal tissues. *Jpn. J. Cancer Res.* **1998**, *89*, 307–314. [[CrossRef](#)] [[PubMed](#)]
66. Allmeroth, M.; Moderegger, D.; Biesalski, B.; Koynov, K.; Rösch, F.; Thews, O.; Zentel, R. Modifying the body distribution of HPMA-based copolymers by molecular weight and aggregate formation. *Biomacromolecules* **2011**, *12*, 2841–2849. [[CrossRef](#)]
67. Allmeroth, M.; Moderegger, D.; Gundel, D.; Buchholz, H.G.; Mohr, N.; Koynov, K.; Rosch, F.; Thews, O.; Zentel, R. PEGylation of HPMA-based block copolymers enhances tumor accumulation in vivo: A quantitative study using radiolabeling and positron emission tomography. *J. Control. Release* **2013**, *172*, 77–85. [[CrossRef](#)]
68. Deshantri, A.K.; Varela Moreira, A.; Ecker, V.; Mandhane, S.N.; Schiffelers, R.M.; Buchner, M.; Fens, M. Nanomedicines for the treatment of hematological malignancies. *J. Control. Release* **2018**, *287*, 194–215. [[CrossRef](#)]
69. Sarin, H. Physiologic upper limits of pore size of different blood capillary types and another perspective on the dual pore theory of microvascular permeability. *J. Angiogenesis Res.* **2010**, *2*, 1–19. [[CrossRef](#)]
70. Cramers, P.; Ruevekamp, M.; Oppelaar, H.; Dalesio, O.; Baas, P.; Stewart, F.A. Foscan uptake and tissue distribution in relation to photodynamic efficacy. *Br. J. Cancer* **2003**, *88*, 283–290. [[CrossRef](#)]
71. Gomer, C.J.; Dougherty, T.J. Determination of [³H]- and [¹⁴C] hematoporphyrin derivative distribution in malignant and normal tissue. *Cancer Res.* **1979**, *39*, 146–151.

72. Reshetov, V.; Lassalle, H.P.; Francois, A.; Dumas, D.; Hupont, S.; Grafe, S.; Filipe, V.; Jiskoot, W.; Guillemin, F.; Zorin, V.; et al. Photodynamic therapy with conventional and PEGylated liposomal formulations of mTHPC (temoporfin): Comparison of treatment efficacy and distribution characteristics in vivo. *Int. J. Nanomed.* **2013**, *8*, 3817–3831. [[CrossRef](#)] [[PubMed](#)]
73. Svensson, J.; Johansson, A.; Grafe, S.; Gitter, B.; Trebst, T.; Bendsoe, N.; Andersson-Engels, S.; Svanberg, K. Tumor selectivity at short times following systemic administration of a liposomal temoporfin formulation in a murine tumor model. *Photochem. Photobiol.* **2007**, *83*, 1211–1219. [[CrossRef](#)] [[PubMed](#)]



© 2020 by the authors. Licensee MDPI, Basel, Switzerland. This article is an open access article distributed under the terms and conditions of the Creative Commons Attribution (CC BY) license (<http://creativecommons.org/licenses/by/4.0/>).